MASTER'S THESIS
DIPLOMARBEIT

EXPERIMENTAL DETERMINATION OF THE STIFFNESS EVOLUTION OF YOUNG CEMENT PASTES WITH AND WITHOUT FLY-ASH AS CEMENT REPLACEMENT MATERIAL

EXPERIMENTELLE BESTIMMUNG DER STEIFIGKEITSENTWICKLUNG JUNGER ZEMENTSTEINE MIT UND OHNE FLUGASCHE ALS ZEMENTERSATZMATERIAL

ausgeführt zum Zwecke der Erlangung des akademischen
Grades eines Diplom-Ingenieurs

unter der Leitung von
Assoc.-Prof. Dipl.-Ing. Dr. techn. Bernhard Pichler
Institut für Mechanik der Werkstoffe und Strukturen

eingereicht an der Technischen Universität Wien
Fakultät für Bauingenieurwesen

von

Philipp Karte
Matrikelnummer: 07 25 387
Kreuzgasse 6/18, 1180 Wien, Österreich

Wien, am 27. Februar 2014 . . . .

Danksagung

Kurzfassung

Um CO_2 Emissionen zu reduzieren, versucht die Zement- und Betonindustrie, klassischen Zement teilweise durch Ersatzmaterialen wie z. B. Flugasche zu ersetzen. Das Ergebnis sind so genannte *verschnittene Zemente*. Mischt man sie mit Wasser, so entsteht ein neuartiger Zementleim, der nach wenigen Stunden zu Zementstein abbindet und anschließend über Wochen, Monate und Jahre hinweg aushärtet. Die mechanischen Eigenschaften dieser neuen Materialien sind allerdings insbesondere in den ersten Tagen nach der Materialherstellung weitestgehend unerforscht. Das ist die Motivation für die vorliegende Arbeit. Es wird die Steifigkeitsentwicklung von Zementsteinen am zweiten, dritten und vierten Tag nach ihrer Herstellung untersucht. Drei verschiedene Materialien werden charakterisiert. Sie unterscheiden sich in der Materialrezeptur, die mit Hilfe des Wasser-Zement-Massenverhältnisses w/c und des Wasser-Bindemittel-Massenverhältnisses w/s angegeben werden. Die Studie beinhaltet zwei klassische Zementsteine, mit $w/c = w/s = 0{,}50$ und $w/c = w/s = 0{,}42$. Weiters wird ein Flugaschenzement untersucht, der aus 16 Massenprozent Flugasche und 84 Massenprozent klassischem Zement besteht: $w/c = 0{,}50$ und $w/s = 0{,}42$. Drei verschiedene Testmethoden werden verwendet. Entlastungsmoduln werden mit Hilfe zerstörungsfreier Druckversuche bestimmt. Dabei kommt eine neue Testmethode zum Einsatz, die sich durch überbestimmte Verformungsmessung auszeichnet. Dynamische Elastizitätsmoduln werden mit Ultraschalltests bestimmt. Differentalkalorimetrie erlaubt es schließlich, einen Zusammenhang zwischen der beobachteten *zeitabhängigen* Frühzeitsteifigkeitsentwicklung und dem Hydratationsgrad herzustellen. Damit wird gezeigt, dass sowohl die Entlastungsmoduln als auch die dynamischen Elastizitätsmoduln aller drei Materialien praktisch linear mit wachsendem Hydratationsgrad ansteigen. Flugasche greift in den ersten Tagen nach der Materialherstellung nicht wesentlich in die auf der Mikrostruktur ablaufenden chemischen Reaktionen ein. Flugaschenpartikel wirken daher als quasi-inerte Bestandteile der Mikrostruktur, die allerdings zu einer Versteifung des Materials beitragen.

Die entwickelte Testmethode wurde am 30. Danubia Adria Symposium (DAS) vorgestellt, das von 25.-28. September 2013, in Primošten, Kroatien, stattfand. Nach dem Symposium wurden wir vom wissenschaftlichen Komitee der Danubia Adria Gesellschaft eingeladen, einen entsprechenden wissenschaftlichen Artikel bei der Zeitschrift *Strain*, einem internationalen Journal für experimentelle Mechanik, ISSN: 1475-1305, einzureichen. Das erfolgte am 10. Februar 2014, siehe (Karte et al., 2014). Die Kapitel 1 bis 6 dieser Diplomarbeit sind dem eingereichten Aufsatz entnommen.

Abstract

In order to reduce CO_2 emissions, cement clinker is nowadays partly replaced by supplementary cementitious materials such as fly ash, but the early-age mechanical performance of blended binders is not as well understood as the one of pure cements. This provides the motivation to study the stiffness evolution of pure and fly ash-blended cement pastes during the second, third, and fourth day after production. Herein, we analyze three material compositions, defined in terms of the initial water-to-cement mass ratio w/c and the initial water-to-solid (binder) mass ratio w/s. Pure cement pastes exhibit $w/c = w/s = 0.50$ and $w/c = w/s = 0.42$, respectively. The fly ash-blended cement paste refers to a cement mass replacement level of 16 percent, and this is related to $w/c = 0.50$ and $w/s = 0.42$. These materials are analyzed by means of three test methods. Unloading modulus is determined using a novel setup for nondestructive uniaxial compression testing including overdetermined deformation measurements. Dynamic Young's moduli are obtained from ultrasonics experiments. Isothermal differential calorimetry allows for linking the observed temporal evolution of early-age stiffness to the hydration degree of cement. Both unloading moduli and dynamic Young's moduli of all three materials increase practically linearly with increasing hydration degree. Fly ash does not contribute significantly to the early-age hydration of the material, i.e. it represents a quasi-inert part of the material's microstructure, exhibiting a significant stiffening effect.

The testing method developed within this master's thesis was presented at the 30th Danubia Adria Symposium (DAS), September 25-28, 2013, Primošten, Croatia. After the meeting, we were invited, by the scientific committee of the Danubia Adria Society, to submit a manuscript to "Strain", an international Journal for Experimental Mechanics, ISSN: 1475-1305. The document was submitted for review and possible publication on Feb 10, 2014, see also reference (Karte et al., 2014). Sections 1 to 6 of this master's thesis essentially reproduce this submitted document.

Contents

Chapter **1**

Introduction

The cement and concrete industry strives for reducing the CO_2 emissions associated with the production of their binders. One strategy is to partly replace traditional cement clinker by supplementary cementitious materials, such as the waste products fly ash or slag (Gartner, 2004). While traditional cements have been developed and optimized over decades, new products must be developed much faster, and this creates rather urgent research need. Blended cements, namely, will be used in the daily construction practice only if they exhibit a similarly predictable performance as traditional cements. This concerns not only the long-term behavior, but also the early-age performance, because speed-up of concrete construction is closely related to the question how soon formworks may be removed, and the answer is related to the interval of time which is required for the binder to develop suitable mechanical properties. This provides the motivation for the current contribution which focuses on the early-age stiffness evolution of pure and fly ash-blended cement pastes. Two independent test methods, mechanical unloading and ultrasonics, respectively, provide access to the stiffness evolution during the second, third, and fourth day after production. Isothermal differential calorimetry allows for linking the observed temporal evolution of early-age stiffness to a maturity parameter quantifying the hydration degree of cement.

The thesis is structured as follows. The composition of the analyzed materials as well as the production technique for specimens for stiffness characterization are described in Section 2. A novel test setup for nondestructive uniaxial compression testing and a related testing procedure for early-age characterization of unloading modulus represent the main original contributions, see Section 3. The calorimetry-based link between material age and hydration degree is the focus of Section 4. Complementary ultrasonics experiments providing access to the early-age evolution of dynamic Young's modulus are described in

Section 5. The thesis closes with a concluding section.

Chapter 2

Pure and fly ash-blended cement pastes

Our analyses involve cement pastes with three different compositions, based on a cement of type CEM I 42.5 N, a commercially available fly ash, and distilled water. The compositions are defined in terms of the initial water-to-cement mass ratio w/c and the initial water-to-solid (binder) mass ratio w/s.

- Paste 1 is produced from cement and water only, with $w/c = w/s = 0.50$. This is representative for compositions used in building construction. Such a superstoichiometric mix contains more water than necessary to (theoretically) hydrate all cement clinker.

- Paste 2 is produced from cement and water only, with $w/c = w/s = 0.42$. This stoichiometric mix contains as much water as is foreseen by the Powers-Acker hydration model (Powers and Brownyard, 1948; Acker, 2001) to be necessary and sufficient to (theoretically) hydrate all cement clinker.

- Paste 3 is a fly ash-blended cement paste exhibiting $w/c = 0.50$ (compare with Paste 1) and $w/s = 0.42$ (compare with Paste 2), i.e. the mass of the solid constituents is composed of 16% fly ash and of 84% cement.

Cylindrical specimens for stiffness characterization are produced by mixing suitable masses of cement, water, and fly-ash, according to the following procedure. The raw materials are mixed for one minute in a mixer. During the subsequent minute, the suspension is hand-mixed with a spoon, in order to ensure homogeneity of the mix even close to the

surface of the mixing bowl. This is followed by another minute of mixing with the mixer. Subsequently, the bowl is dynamically excited on a vibration table, to remove possibly entrapped air from the paste. Finally, we let the material slide – over an extended funnel – into an inclined mold. During this action, the mold is placed on the vibrating table, separated from the latter with a sponge, such that the effective vibration energy can be controlled by the force with which the mold is pressed against the sponge. For more details regarding practical steps used for the casting process, see Appendix B.1.

The cylindrical specimens exhibit a diameter $d = 30\,\text{mm}$ and a height $h = 150\,\text{mm}$. They are cured in an upright position, inside a climate chamber conditioned to 20 degrees centigrade and to a relative humidity amounting to 95 percent. In order to avoid significant loss of water by means of vaporization, the samples are always sealed against the ambient air, apart from short-term handling operations such as demolding, surface treatments, dimensioning, and weighing, described next. The samples are typically demolded 23 hours after production. This is followed by surface treatment aiming (i) at removing zones which might be affected by segregation effects, both from the bottom and from the top of the specimens, and (ii) at achieving co-planarity of the two circular end surfaces. The best method for these tasks turned out to be careful shaving with a Stanley knife, because standard procedures such as grinding could be shown to damage the tested materials measurably. For more details regarding sample handling prior to testing, see Appendix B.

Chapter 3

Unloading in uniaxial compression

A uniaxial compression experiment complying with scientific accuracy standards requires loading by means of close-to-perfect uniform normal tractions, raising the need for a central load application and consideration of friction in the interfaces between specimen and load plates, see, e.g., (Amieur, 1994) for a review of classical methods. Mechanical testing of cement pastes at *early ages* further increases the testing complexity, because the materials are very fragile and prone to be damaged by virtually any handling operation, see, e.g., the early-age testing activities described in (Pichler et al., 2013; Fischer et al., 2014). In order to deal with these challenges, we here describe a novel test setup and a related testing procedure for early-age mechanical stiffness characterization by means of repeated unloading. Overdetermined displacement measurements turn out to be very beneficial for ensuring high-quality testing. For more details regarding the theoretical background of mechanical unloading testing, see Appendix A.1.

3.1 Test setup

A uniaxial compression experiment requires loading by means of *uniform* normal tractions, raising the need for a central load application (Amieur, 1994). Any undesired eccentricity of the loading induces stress and strain gradients inside the specimen, contradicting the homogeneous stress and strain fields required for a *material* test. We here achieve close-to-perfect centricity of the loading by means of the following novel setup. We use a serial arrangement of the specimen with other elements, including two metal cylinders exhibiting so called bottlenecks: one above and one below the specimen (Fig. 3.1). The bottlenecks exhibit a diameter of $3\,\mathrm{mm}$, and this is one order of magnitude smaller than the diameter of

the sample, which amounts to 30 mm (Fig. 3.1). The applied force is transmitted through
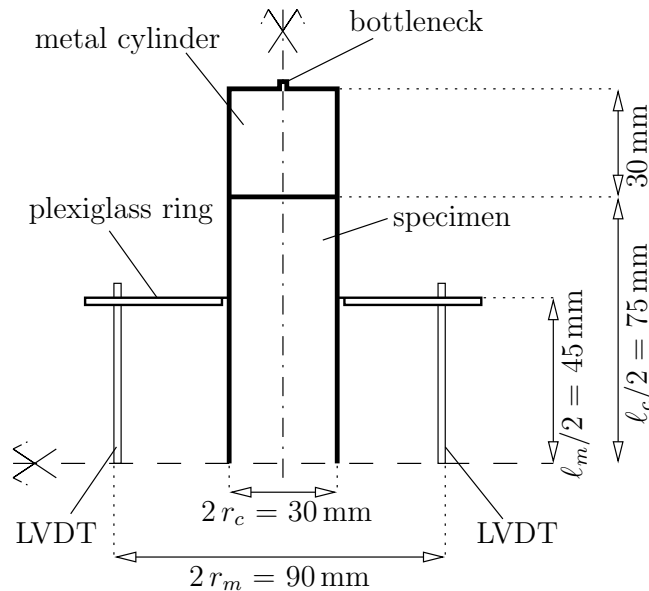
Figure 3.1: Symmetric upper half of the test setup consisting of a metal cylinder with a bottleneck, the cylindrical specimen, and a plexiglass ring holding five LVDTs which are evenly distributed around the perimeter of the specimen

the entire serial arrangement and, hence, also across the two bottlenecks, such that the loading represents in very good approximation a "point loading" there. Connecting the two loading points by a straight line defines the axis of loading, and our setup is chosen such that the axis of the cylindrical specimen coincides with the axis of loading.

Loading by means of uniform normal tractions is achieved through the steel cylinders which are directly attached to the specimen. They widen the stress trajectories from the end with the bottleneck, to a homogeneous load distribution at the other end, where the metal cylinder is in contact with the specimen. Still, metal and cement paste exhibit different Poisson's ratios. This induces – under compressive axial loading – incompatible lateral displacements in the metal-specimen interfaces, resulting in friction-induced shear stresses acting in these interfaces. They render the stress field inside the specimen inhomogeneous and multiaxial, contradicting the desired uniform and uniaxial compressive stress state. Notably, the principle of Saint Venant (Barré de Saint Venant, 1855) implies that the self-equilibrated shear stresses decrease with increasing distance from the metal-specimen interfaces, such that they reach insignificant magnitudes in a distance amounting to one times the diameter of the specimen. In other words, the top and bottom 30 mm of the specimen must be expected to be affected by the undesired and hardly measurable shear stresses, such that these regions are actually to be interpreted as a part of the load appli-

cation setup. Outside these boundary domains, i.e. in the central part of the specimen, in turn, a uniaxial stress state free of significant shear stresses can be expected.

Accurate deformation quantification requires measurements directly on the sample. Herein, we use five Linear Variable Differential Transducers (LVDTs) of type "Solartron", measuring the relative displacement between two plexiglass rings which are fixed – in a distance of 90 mm – to the aforementioned central part of the specimen (Fig. 3.1). The plexiglass rings are clamped to the specimen such that a continuous contact around the specimen's diameter is established. The five LVDTs are evenly distributed around the perimeter of the specimen. Noting that three LVDTs would be sufficient to measure the relative movement of the two plexiglass rings, our setup with five LVDTs ensures an overdetermined (and, hence, redundant) mode of measurements, significantly increasing the measurement accuracy.

Also during mechanical testing, the samples are conditioned to 20 degrees centigrade, because they are still undergoing the chemical hydration process which is temperature-activated such that the speed of hydration increases with increasing temperature and vice versa. To this end, the described test setup was placed inside an insulated temperature chamber, conditioned with a temperature control unit "Lauda RK8 KP". For a more detailed description of the practical steps associated with mechanical unloading, see Appendix B.2.

3.2 Prescribed loading history

Three loading-unloading cycles are performed every hour, with help of an electromechanical universal testing machine of type "Walter and Bai LFM 150". During the remaining part of every hour, a permanent compressive force amounting to 0.05 kN ensures that the whole setup (including the sample and the bottlenecks) stays in an upright position without tipping over. All loading and unloading events are carried out under force control, with a desired force rate amounting to 1 kN/s, corresponding to a cement paste-related stress rate amounting to 1.41 MPa/s. Subsequent load level changes are separated from each other by a waiting period amounting to 20 s. First, the compressive load level is increased from the permanent load level up to 0.10 kN (0.14 MPa). This is followed by three loading-unloading cycles up to 0.40 kN (0.57 MPa) and back to 0.10 kN (Fig. 3.2). Finally, the load level is reduced back to the permanent load level.

The PID control settings of the testing machine is chosen such as to maximize the central part of each unloading event, in which the desired force rate (1 kN/s) was actually reached, i.e. to minimize the durations of the initial acceleration period and of the final

deceleration period (Fig. 3.2(b)). The optimum PID setup results in overshooting the upper load level (0.40 kN) up to 0.45 kN (0.64 MPa) and of undershooting the lower load level (0.10 kN) down to 0.08 kN, but the force never fell significantly below the permanent load level (0.05 kN) which ensured to keep the setup in the desired position.
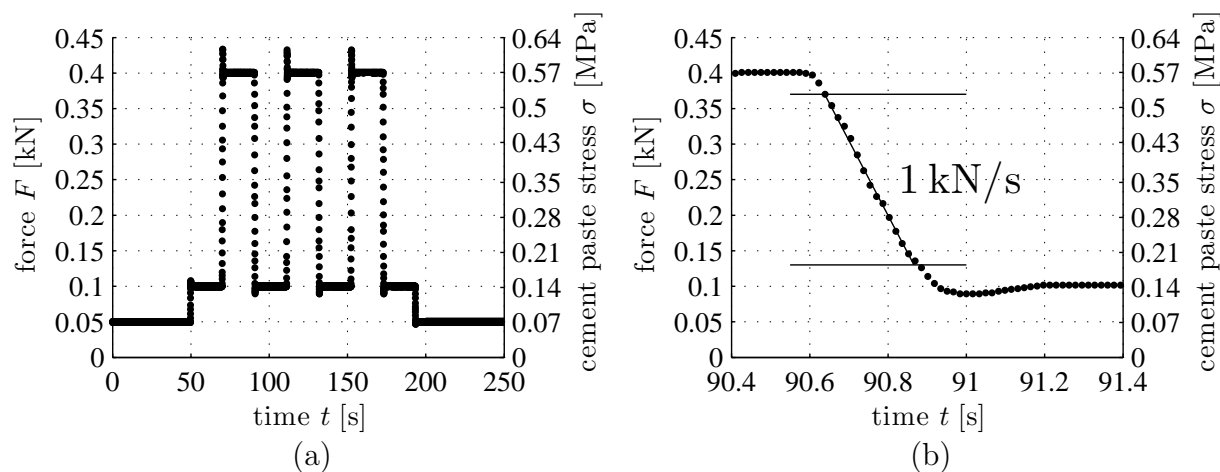
Figure 3.2: Loading history: (a) overview over testing program repeated every hour, essentially consisting of three compressive loading-unloading cycles between 0.10 kN and 0.40 kN, and (b) details of the first unloading, highlighting the central region where the desired unloading speed amounting to 1 kN/s is realized

The described loading history ensures (i) nondestructive testing, (ii) at a virtually constant microstructure of the sample, (iii) with a minimum influence of creep on the unloading behavior, but (iv) still suitably large deformations such that the LVDT measurements are reliable. These aspects are discussed next. As for (i), we note that the maximum compressive load, 0.45 kN, corresponds to a compressive normal stress of 0.64 MPa, and this is smaller than 30 percent of the uniaxial compressive strength of the tested materials at any time of testing. In other words, the tests stay out of the so-called nonlinear creep regime (Ruiz et al., 2007), which would result in damage of the material (Rossi et al., 2012; Fischer et al., 2014). As for (ii), we emphasize that one set of three unloading cycles is finished within 150 seconds. During this period of time, the chemical hydration process does not make significant progress, such that all three unloading events refer to practically the same microstructure. As for (iii), it is noteworthy that each individual unloading event is practically finished within two tenths of a second. This is so short that time-dependent creep deformations do not contribute significantly to the unloading deformations. As for (iv), we note that the unloading-induced elongation of the specimens is typically larger than 5 microns, and this is significantly larger than 1 micron which is the expected measurement

accuracy of the used LVDTs.

3.3 Data acquisition

The measurement signals of the five LVDTs (Fig. 3.3) together with the signal from the force measurement unit of the universal testing machine (Fig. 3.2(a)) are processed and stored inside Excel sheets with help of the digital measurement equipment "Orbit" of "Solartron Metrology". A visual basic script controls the measurement frequency: during the loading-unloading cycles, 70 individual readings are taken every second; during the rest of the hour (permanent load level), the measurement frequency is reduced to one reading every two seconds.
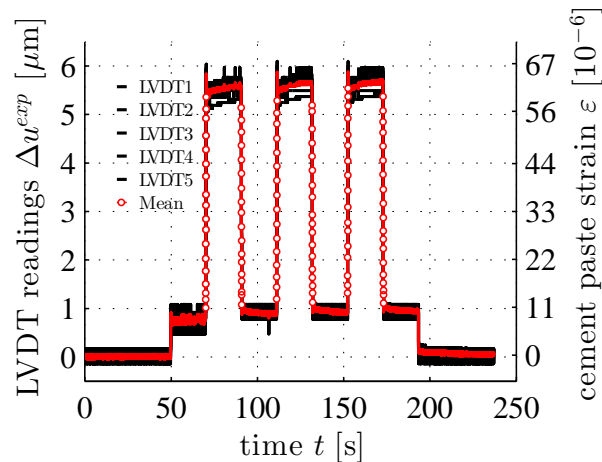
Figure 3.3: Typical measurements of the five LVDTs and their mean values (see circles), after minimization of loading eccentricity

3.4 Minimization of loading eccentricity

The five LVDTs do not deliver exactly the same readings. The deviation of individual LVDT readings from their mean stems from an effective eccentricity of the applied normal force. Therefore, the LVDT readings are used for fine-tuning the position of the test setup, in order to minimize loading eccentricity.

As for quantification of the effective eccentricity of the applied normal force, we evaluate our deformation measurements based on first-order beam theory, i. e. the specimen part between the two plexiglass rings is idealized as a simply supported beam with axial coordinate x. The beam is loaded, at both ends, by a compressive normal force F exhibiting an eccentricity e in the negative z-direction, see Fig. 3.4. Therefore, both the normal
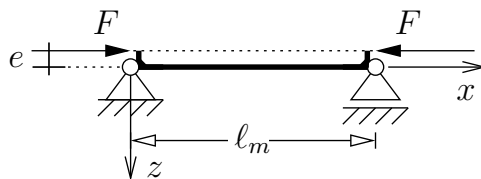
Figure 3.4: Model for the central part of the specimen, located between the two plexiglass rings: simply supported beam subjected to a normal force F exhibiting an eccentricity e in the negative z-direction

force N and the bending moment M are constant along the beam

$$N(x) = -F, \qquad M(x) = F\,e \tag{3.1}$$

The field of the axial displacement component reads, according to first-order beam theory, as

$$u(x,z) = -\frac{F\,x}{EA} - \frac{F\,e}{EI}\left(\frac{l_0}{2} - x\right)z \tag{3.2}$$

where E stands for Young's modulus and where $EI = E\,r_c^4\,\pi/4$ as well as $EA = E\,r_c^2\,\pi$, respectively, stand for the bending stiffness and for the extensional stiffness of the cylindrical specimen. The beam-theoretical analogon to the measurements of the i-th LVDT is obtained by calculating the difference of the axial displacements between $x = 0$ and $x = \ell_m$, i.e. $\Delta u^{mod}(z) = u(x=0, z) - u(x=\ell_m, z)$, and by specifying the resulting expression for the z-coordinate of the i-th LVDT: $z_i = r_m\,\cos(\phi_i)$; this delivers

$$\Delta u_i^{mod} = \frac{F\,\ell_m}{EA}\left[1 - \frac{e\,r_m\,\cos(\phi_i)}{i^2}\right] \tag{3.3}$$

where i denotes the radius of inertia of the cylinder cross-section ($i^2 = I/A$), and where the polar angles ϕ_i with $i \in \{1, 2, 3, 4, 5\}$ follow from $\phi_i = \phi_1 + (i-1)\,2\pi/5$. The two unknowns model quantities, i.e. the eccentricity e and the polar angle of the first LVDT, ϕ_1, are identified through minimization of the sum of the squared differences between measured length changes Δu_i^{exp} and modeled length changes Δu_i^{mod}:

$$\sum_{i=1}^{5}\left[\Delta u_i^{exp} - \Delta u_i^{mod}\right]^2 \to \min \tag{3.4}$$

Magnitude and orientation of the effective eccentricity allow us to fine-tune the position of our test setup. This way, the effective eccentricity is incrementally reduced down to magnitudes of typically 0.1 mm, see Fig. 3.3 for corresponding LVDT readings which scatter only marginally around their mean. Once a close-to-optimal position of our test setup is found, the described automatic testing procedure is started, typically 24 h after sample production. For a more detailed calculation of the effective load eccentricity, see Appendix B.2.1

3.5   Test evaluation and results

Unloading modulus is determined from point-wisely defined stress-strain-diagrams. The stress ordinates are obtained from dividing the force readings by the cross-sectional area of the cylindrical specimens, $A = 7.07\,\mathrm{cm}^2$ (see the right ordinates in Fig. 3.2). As for the required strain ordinates, the average over the five individual LVDT readings is divided by the LVDT measurement length, i.e. by the 90 mm distance of the two plexiglass rings (see the right ordinate in Fig. 3.3). Plotting stress values as a function of corresponding strain values delivers a chain of data points, which can be very accurately fitted by a straight line, the slope of which represents the sought unloading modulus (Fig. 3.5).
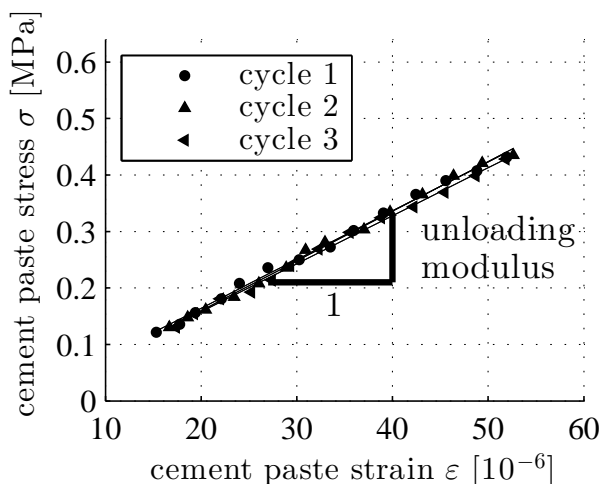
Figure 3.5: Point-wisely defined stress-strain-diagrams referring to three unloading cycles: the slope of best linear fits to the chains of data points represents the sought unloading modulus

Our measurements allow us to evaluate three unloading moduli every hour. They show a very small scatter (Fig. 3.5), indicating a high reproducibility of our tests. Their average value represents the output of each set of three loading-unloading cycles. Plotting these mean values as a function of the age of the materials (Fig. 3.6) underlines that hydration-induced stiffening of the tested materials is underlinear during the second, third, and fourth day after production.

For each type of paste, a test repetition was carried out (Fig. 3.6). The evaluated unloading moduli exhibit very satisfactory small differences, underlining the repeatability of our experiments. For raw data of Fig. 3.6 see Tables D.1, D.2, D.5, D.6, D.9, and D.10 in Appendix D.
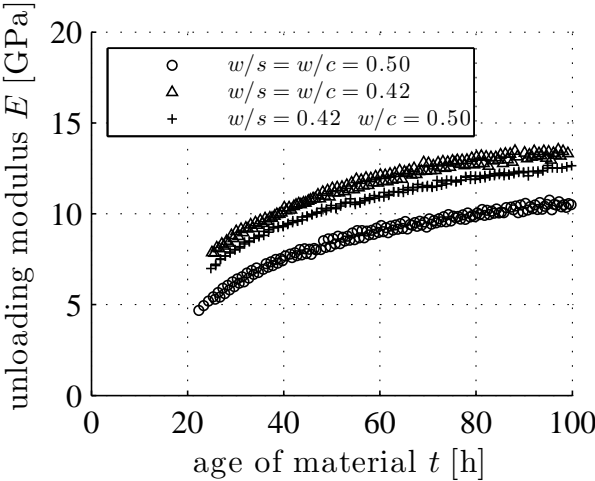
Figure 3.6: Temporal evolution of unloading modulus of the tested cement pastes; paste 1: circles, paste 2: triangles, fly ash-blended paste 3: crosses

Chapter 4

Isothermal Differential Calorimetry

In order to establish a relation between the age of the tested materials and the maturity of their microstructures, isothermal differential calorimetry measurements are carried out at 20 degrees centigrade. Each individual test involves a test tube containing 10 g solid binder and a separated syringe filled with the required amount of distilled water. Both elements are put into a testing cell of a calorimeter "ToniCAL Trio type 7339". Once a stationary temperature regime is reached (20 degrees centigrade), the test is started by injecting the water to the binder and by mixing the paste using a plastic paddle. Notably, both actions are carried out without re-opening the test cell. The primary measurement result is the accumulated heat release $Q(t)$, determined during the first four days after mixing, see Fig. 4.1. Two tests are carried out for each of the three types of pastes. The similarity of results obtained with the same composition indicates a satisfactory reproducibility of the experiments.

Fly ash is well known to exhibit a very small reactivity which is practically negligible during the first days after material production (Lothenbach et al., 2011). This suggests that the observed hydration of the fly ash-blended cement paste stems practically speaking from the cement content only.

As to quantify the relation between material age and microstructural maturity, a calorimetry-based estimate of the cement-related hydration degree ξ is determined. To this end, the averaged accumulated heat release $Q(t)$ is divided through the mass of cement ($m_c = 10$ g for pastes 1 and 2, and $m_c = 8.4$ g for the fly ash-blended paste 3) and the result is divided through $\ell_h = 500$ J/g which is – in very good approximation – equal
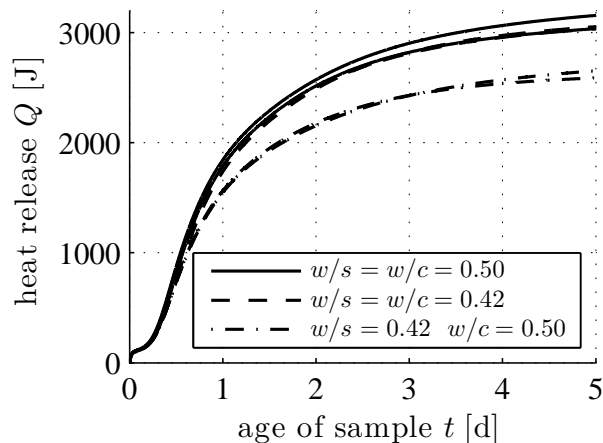
Figure 4.1: Temporal evolution of accumulated heat release measured in isothermal differential calorimetry with 10 g solid binder and suitable amounts of distilled water; paste 1: solid lines, paste 2: dashed lines, fly ash-blended paste 3: dash-dotted lines

to the latent heat of typical CEM I cements (Byfors, 1980; Taylor, 1990)

$$\xi(t) = \frac{Q(t)}{m_c \, \ell_h} \tag{4.1}$$

The described hydration degree increases nonlinearly with time (Fig. 4.2), and all three pastes exhibit virtually the same evolution. This corroborates the expectation that fly ash
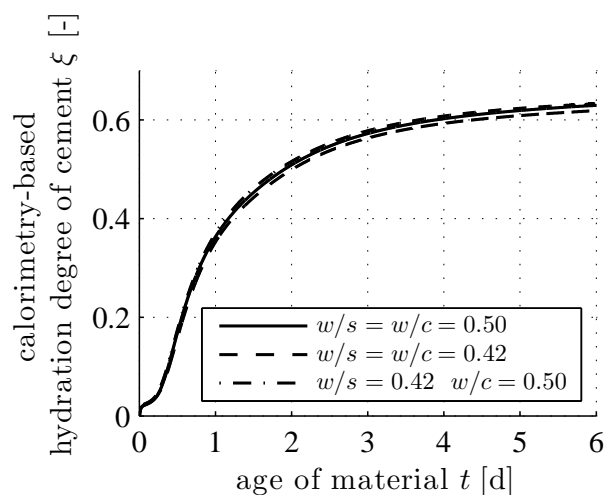
Figure 4.2: Temporal evolution of calorimetry-based hydration degree of cement according to Eq. (4.1) with $Q(t)$ take from Fig. 4.1: paste 1: solid line, paste 2: dashed line, fly ash-blended paste 3: dash-dotted line

does not contribute significantly to chemical reactions at the microscale of paste 3. This

is consistent with other observations (Lothenbach et al., 2011) in which it was found that fly ash hydration is hardly reactive at very early ages. In other words, fly ash particles act as practically inert parts of the cement paste microstructure during the performed tests.

Unloading modulus as a function of calorimetry-based hydration degree is obtained from combining the mechanical test data "unloading modulus as a function of material age" with the calorimetry test data "hydration degree as a function of material age". Unloading moduli of all three analyzed mixes increase practically linearly with increasing hydration degree (Fig. 4.3). Detailed information about the performance of calorimetry
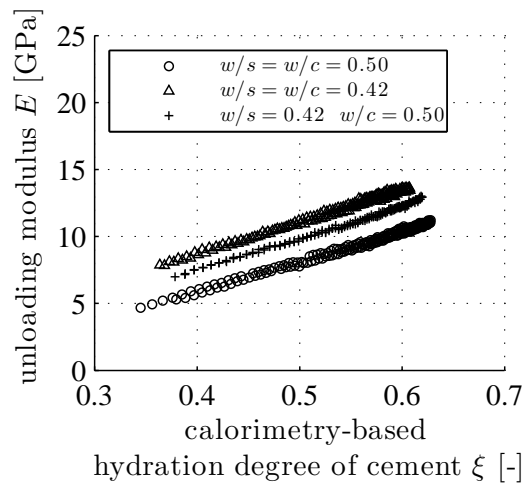
Figure 4.3: Unloading modulus as a function of calorimetry-based hydration degree of cement: paste 1: circles, paste 2: triangles, fly ash-blended paste 3: crosses

testing can be found in Appendix C. This section summarizes the main results of (Karte, 2013).

Chapter 5

Ultrasonics experiments

Ultrasonics experiments provide an independent access to the stiffness of the analyzed cement pastes, namely, to so-called *dynamic* elastic properties. Using an ultrasound frequency amounting to 250 kHz, longitudinal and shear waves are sent through the produced specimens, using a "Panametrics-NDT" equipment. Dividing the cylinder length (= wave travel distance) through the time required for the ultrasound waves to travel through the specimen (= primary measurement result) delivers longitudinal wave speeds v_ℓ and transversal wave speeds v_t, both of which increase with increasing age of the material (Fig. 5.1).
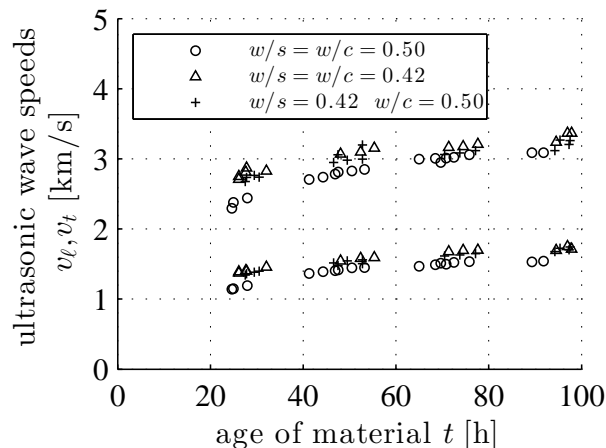
Figure 5.1: Ultrasound wave speeds as a function of material age; paste 1: circles, paste 2: triangles, fly ash-blended paste 3: crosses

In each test, the wave length λ is obtained from dividing wave speed through the used ultrasound frequency. Notably, the wave lengths were, any time, larger than 4 mm. This underlines that the separation of scales principle (Kohlhauser and Hellmich, 2013) was satisfied, i. e. the wavelength values are significantly larger than the size of the representative cement paste volume, amounting to 250 μm; and this is again sufficiently larger than the characteristic size of heterogeneity of the material, which is equal to the characteristic diameter of clinker grains, amounting to 50 μm.

As for determination of dynamic Young's modulus E_{dyn}, the measured wave velocities are combined with the mass density ρ of the samples, according to the following relation from the theory of elastic waves traveling through an isotropic elastic body (Kolsky, 1963)

$$E_{dyn}(\rho, v_t, v_\ell) = \frac{\rho v_t^2 (3v_\ell^2 - 4v_t^2)}{v_\ell^2 - v_t^2} \tag{5.1}$$

Combining ultrasonics results with calorimetry results implies that dynamic Young's moduli increase practically linearly with increasing hydration degree (Fig. 5.2). This is consistent with observations of Boumiz et al. (Boumiz et al., 1996), carried out during the first 24 hours after material production, and with observations by Helmuth and Turk (Helmuth and Turk, 1966), carried out on mature cement pastes, six to 24 months after their production.
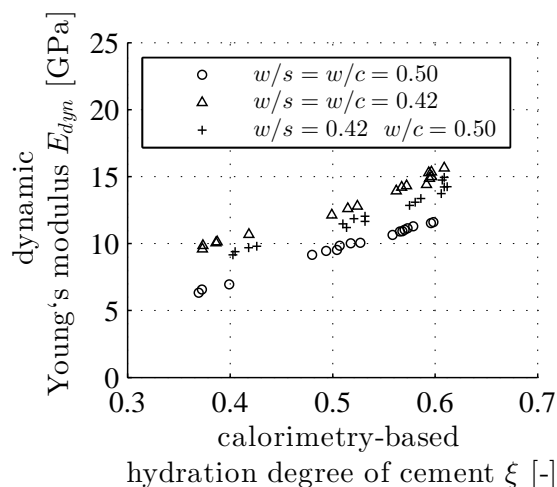
Figure 5.2: Dynamic Young's modulus as a function of calorimetry-based hydration degree of cement: paste 1: circles, paste 2: triangles, fly ash-blended paste 3: crosses

For detailed description of the theoretical background of ultrasonics testing, see Appendix A.2. The practical steps for ultrasonics testing performance are described in Appendix B.3. For raw data of Fig. 5.2, see Tables D.3, D.4, D.7, D.8, D.11, and D.12 in Appendix D

Chapter 6

Summary and conclusions

We here studied both unloading modulus and dynamic Young's modulus of cement pastes as functions of calorimetry-based hydration degree. Two pure and one fly ash-blended cement paste were characterized during the second, third, and fourth day after production.

As far as the early-age stiffness evolution is concerned, we draw the following conclusions:

- Early-age stiffness of pure and blended cement pastes increases practically linearly with increasing hydration degree.

- The ultrasound-related dynamic Young's moduli are, 24 hours after production, by 21 percent ($w/c = w/s = 0.42$), by 25 percent ($w/c = 0.5$, $w/s = 0.42$), and by 29 percent ($w/c = w/s = 0.5$) larger than the corresponding unloading moduli derived from uniaxial compression experiments with an unloading stress rate amounting to $1.41\,\mathrm{MPa/s}$. The described ratio reduces monotonously with increasing age of the materials and reaches typical values of 11 to 12 percent, four days after production.

- The difference between dynamic Young's moduli and unloading moduli is likely related to the behavior of water, including the activation of pore pressures in ultrasound testing (Venkovic et al., 2013). This underlines the complexity of cementitious materials, because a similar effect is typically unknown for other media, including tissue engineering scaffolds (Luczynski et al., 2013).

- The stiffness evolution of a fly ash-blended cement paste with initial water-to-solid mass ratio $w/s = 0.42$ and initial water-to-cement mass ratio $w/c = 0.50$ falls between the stiffness evolution of a pure cement paste exhibiting $w/c = w/s = 0.42$

and the one of a pure cement paste exhibiting $w/c = w/s = 0.50$. Since fly-ash particles exhibit a significant stiffening effect the stiffness evolution of the blended cement paste is closer to the one of the paste exhibiting $w/c = w/s = 0.42$.

As far as the hydration kinetics are concerned, we draw the following conclusions:

- During the first four days after production, all three materials exhibit virtually the same cement-related hydration degree, i.e. fly ash particles represent quasi-inert constituents of the microstructure of cement paste.

- At the analyzed blend level of 16 percent of the cement mass, fly-ash does not exhibit a significant "filler effect" (Lothenbach et al., 2011), i.e. the presence of fly ash particles does not significantly increase the speed of cement hydration by providing preferred nucleation sites for precipitation of calcium silicate hydrates.

Chapter 7

Bibliography

Acker, P. (2001). Micromechanical analysis of creep and shrinkage mechanisms. In *Creep, Shrinkage and Durability Mechanics of Concrete and Other Quasi-brittle Materials*, pages 15–26, Amsterdam. 6th International Conference CONCREEP@MITElsevier, Ulm F.-J., Bazant Z.P., Wittmann F.H. (Eds.).

Amieur, M. (1994). *Etude numérique et expérimentale des effets d'échelle et de conditions aux limites sur des éprouvettes de béton n'ayant pas le volume représentatif [Numerical and experimental study of scale effects and boundary conditions on concrete specimens having no representative volume]*. Doctoral thesis n°1256, École Polytechnique Fédérale de Lausanne (EPFL), Lausanne. In French. Available online at: https://infoscience.epfl.ch/record/31734?ln=fr.

Barré de Saint Venant, A. J. C. (1855). Mémoire sur la torsion des prismes, [Memory on twisting prisms], Mémoires des Savants étrangers [Memoires of foreign scholars]. *Comptes rendues de l'Académie des Sciencies*, 14:233–560.

Boumiz, A., Vernet, C., and Cohen Tenoudji, F. (1996). Mechanical properties of cement pastes and mortars at early ages. *Advanced Cement Based Materials*, 3(3-4):94–106.

Byfors, J. (1980). Plain concrete at early ages. Technical report, Swedish Cement and Concrete Research Institute, Stockholm, Sweden.

Fischer, I., Pichler, B., Lach, E., Terner, C., Barraud, E., and Britz, F. (2014). Compressive strength of cement paste as a function of loading rate: experiments and engineering mechanics analysis. *Cement and Concrete Research*. Accepted for publication.

Gartner, E. (2004). Industrially interesting approaches to "low-CO$_2$" cements. *Cement and Concrete Research*, 34(9):1489–1498.

Helmuth, R. and Turk, D. (1966). Elastic moduli of hardened Portland cement and tricalcium silicate pastes: Effect of porosity. *Symposium on structure of Portland cement paste and concrete*, 90:135–144. Highway Research Board, Washington, DC.

Karte, P. (2012/2013). Differential calorimetry: Start up testing with a calorimeter tonical trio type 7339. Technical report, Institute for Mechanics of Materials and Structures Vienna University of Technology (TU Wien).

Karte, P., Hlobil, M., Reihsner, R., Dörner, W., Lahayne, O., Eberhardsteiner, J., and Pichler, B. (2014). Early-age stiffness characterization of cement pastes. *Strain.*

Kohlhauser, C. and Hellmich, C. (2013). Ultrasonic contact pulse transmission for elastic wave velocity and stiffness determination: Influence of specimen geometry and porosity. *Engineering Structures*, 47:115–133.

Kolsky, H. (1963). *Stress waves in solids.* Courier Dover Publications.

Lothenbach, B., Scrivener, K., and Hooton, R. D. (2011). Supplementary cementitious materials. *Cement and Concrete Research*, 41(12):1244–1256.

Luczynski, K., Brynk, T., Ostrowska, B., Swieszkowski, W., Reihsner, R., and Hellmich, C. (2013). Consistent quasistatic and acoustic elasticity determination of poly-l-lactide-based rapid-prototyped tissue engineering scaffolds. *Journal of Biomedical Materials Research Part A*, 101(1):138–144.

Pichler, B., Hellmich, C., Eberhardsteiner, J., Wasserbauer, J., Termkhajornkit, P., Barbarulo, R., and Chanvillard, G. (2013). Effect of gel-space ratio and microstructure on strength of hydrating cementitious materials: An engineering micromechanics approach. *Cement and Concrete Research*, 45:55–68.

Pichler, B. and Lahayne, O. (2011/2012). Skriptum zum experimentellen Teil der Übung aus Festigkeitslehre. Technical report, Institute for Mechanics of Materials and Structures Vienna University of Technology (TU Wien).

Powers, T. and Brownyard, T. (1948). *Studies of the physical properties of hardened Portland cement paste*, pages 101–992. Res. Lab. Portland Cem. Assoc. Bull. 22.

Rossi, P., Tailhan, J.-L., Le Maou, F., Gaillet, L., and Martin, E. (2012). Basic creep behavior of concretes investigation of the physical mechanisms by using acoustic emission. *Cement and Concrete Research*, 42(1):61–73.

Ruiz, M., Muttoni, A., and Gambarova, P. (2007). Relationship between non-linear creep and cracking of concrete under uniaxial compression. *Journal of Advanced Concrete Technology*, 5(3):383–393.

Taylor, H. (1990). *Cement Chemistry*. Academic Press, New York.

Venkovic, N., Sorelli, L., Sudret, B., Yalamas, T., and Gagn, R. (2013). Uncertainty propagation of a multiscale poromechanics-hydration model for poroelastic properties of cement paste at early-age. *Probabilistic Engineering Mechanics*, 32:5–20.

Appendix A

Theoretical background for mechanical unloading and ultrasonics testing

Stiffness is the resistance against deformation when a material sample is subjected to mechanical loading. Herein, the isotropic stiffness evolution of hydrating cementitious pastes is studied. Thereby, we restrict our considerations to reversible deformation processes and, hence, to *elastic* stiffness.

Knowledge on two independent constants is sufficient to describe the three-dimensional elastic behavior of an isotropic material. Quasi-static mechanical unloading experiments and dynamic ultrasonic measurements were used to identify the two independent material constants. Background information for the experimental measurements is described in the sequel, following the lecture notes (Pichler and Lahayne, 2012).

A.1 Basic principles of mechanical unloading testing

Uniaxial stress is a force density. Therefore, it can be described as

$$\sigma = \frac{F}{A}, \tag{A.1}$$

where F is the force acting on an area A, that can be seen as the undeformed area or the deformed area. Since deformations are very small when investigating cementitious paste samples, both areas are approximately the same and the undeformed cross-sectional area

used in the sequel is a good approximation for the deformed cross-sectional area. The undeformed cross-sectional area A of a cylindrical specimen with diameter d is given as

$$A = \frac{d^2 \pi}{4}. \tag{A.2}$$

Compressive stress (compression) is the stress state caused by an applied load that acts to reduce the length of the material (compression member) in the direction of the applied load. Uniaxial compression testing is characterized by a uniform stress state. Considering that the x_1-axis of a coordinate system is aligned with the force direction, we obtain the following stress state:

$$\boldsymbol{\sigma} = \sigma_{11} \, \mathbf{e}_1 \otimes \mathbf{e}_1 . \tag{A.3}$$

Specifying the inverse Hooke's law,

$$\boldsymbol{\varepsilon} = \mathbf{C}^{-1} : \boldsymbol{\sigma} , \tag{A.4}$$

for the stress state described in (A.3), leads to the strain state for isotropic materials:

$$\boldsymbol{\varepsilon} = \frac{\sigma_{11}}{E} \, \mathbf{e}_1 \otimes \mathbf{e}_1 - \nu \frac{\sigma_{11}}{E} \Big(\mathbf{e}_2 \otimes \mathbf{e}_2 + \mathbf{e}_3 \otimes \mathbf{e}_3 \Big) , \tag{A.5}$$

where E and ν are the Young's modulus and the Poisson's ratio, respectively. By comparing (A.5) with the general components of the linearized strain tensor $\boldsymbol{\varepsilon}$ in a Cartesian coordinate system

$$\boldsymbol{\varepsilon} = \sum_{i=1}^{3} \sum_{j=1}^{3} \varepsilon_{ij} \, \mathbf{e}_i \otimes \mathbf{e}_j , \tag{A.6}$$

allows for identification that all shear strain components are equal to zero and the normal strain components amount to:

$$\varepsilon_{11} = \frac{\sigma_{11}}{E} , \qquad \varepsilon_{22} = \varepsilon_{33} = -\nu \frac{\sigma_{11}}{E} . \tag{A.7}$$

Notably, a uniaxial stress state (A.3) corresponds to a three-axial normal strain state (A.7). Replacing, in Equation (A.7), the indices "11" of the axial stress and the axial strain by "*axial*" and the indices "22" and "33" of the strains perpendicular to the loading direction by "*lateral*" leads to the basic relationship of uniaxial compression:

$$\varepsilon_{axial} = \frac{\sigma_{axial}}{E} , \qquad \varepsilon_{lateral} = -\nu \frac{\sigma_{axial}}{E} . \tag{A.8}$$

Solving the first of the two equations in (A.8) for the Young's modulus yields

$$\frac{\sigma_{axial}}{E} = \varepsilon_{axial} \Rightarrow E = \frac{\sigma_{axial}}{\varepsilon_{axial}} . \tag{A.9}$$

Dividing the lateral strain $\varepsilon_{lateral}$ by the axial strain ε_{axial}, see (A.8), and solving for the Poisson's ratio yields:

$$\frac{\varepsilon_{lateral}}{\varepsilon_{axial}} = \frac{-\nu \dfrac{\sigma_{axial}}{E}}{\dfrac{\sigma_{axial}}{E}} = -\nu \quad \Rightarrow \quad \nu = -\frac{\varepsilon_{lateral}}{\varepsilon_{axial}} \, . \tag{A.10}$$

Equations (A.9) and (A.10) show that the knowledge of the axial stress, the axial strain, and the lateral strain allows for the determination of the Young's modulus and the Poisson's ratio of an isotropic material.

A.2 Basic principles of dynamic ultrasonics experiments

Ultrasonic measurements allow for the stiffness determination of a specimen. Fundamental equations of linear elasticity theory and basic characteristics of wave propagation are described in Sections A.2.1 and A.2.2, respectively. The elastic wave propagation is explained subsequently (Section A.2.3) followed by two examples concerning the longitudinal wave propagation and the shear wave propagation, respectively.

A.2.1 Basic equations of linear elasticity theory

The fundamental equations of linear elasticity theory can be divided into three categories:

1. linear relationships between strain and displacement derivatives; so-called geometric equations

$$\boldsymbol{\varepsilon} = \frac{1}{2} \left[\nabla \mathbf{u} + (\nabla \mathbf{u})^T \right], \tag{A.11}$$

   where $\boldsymbol{\varepsilon}$ is the linearized strain tensor and $\nabla \mathbf{u}$ is the displacement gradient,

2. material equations, characterising the linear elastic material behavior (generalized Hooke's law)

$$\boldsymbol{\sigma} = \mathbf{C} : \boldsymbol{\varepsilon} \,, \tag{A.12}$$

   where $\boldsymbol{\sigma}$ is the stress tensor and $\mathbf{C}$ is the stiffness tensor;

3. and dynamic equilibrium relationships

$$\mathrm{div}\boldsymbol{\sigma} = \rho \, \frac{\partial^2 \mathbf{u}}{\partial t^2} \,, \tag{A.13}$$

   where volume forces were neglected. ρ is the mass density, $\mathbf{u}$ the displacement vector and t the time variable.

A.2.2 Basic characteristics of wave propagation

The relationship between vibration frequency f (unit: $1/s = \text{Hz}$) and angular frequency ω (unit: rad/s) reads as

$$\omega = 2\pi f. \tag{A.14}$$

The relationship between the wave propagation speed v (unit: m/s), wavelength λ (unit: m) and vibration frequency f is given as

$$v = \lambda f. \tag{A.15}$$

Moreover, the wave number k (unit: $1/m$) is indirect proportional to the wave length λ. Given a wave travelling through a solid medium, the relationship between k and λ reads as

$$k = \frac{2\pi}{\lambda}. \tag{A.16}$$

A.2.3 Elastic wave propagation

As to solve the problem of wave propagation in elastic materials, the following ansatz for the displacement is used:

$$\mathbf{u}(\mathbf{x}, t) = \mathbf{A}_0 \cos(\mathbf{k} \cdot \mathbf{x} - \omega t), \tag{A.17}$$

where $\mathbf{A}_0$ is the vectorial form of the amplitude of the material particles displacement components and $\mathbf{k}$ is the vector of the wave propagation direction. Using $\mathbf{n}$ as the unit vector pointing in wave propagation direction, allows for the following representation of the wave vector:

$$\mathbf{k} = k\,\mathbf{n}, \tag{A.18}$$

where the wave number k describes the wave vector length: $k = |\mathbf{k}|$.

In the following, the displacement ansatz (A.17) is inserted into the linear geometric relationships (A.11) and in the dynamic equilibrium relationships (A.13). Subsequently the geometric relationship (A.11) is inserted into the material equation (A.12) and the resulting stress tensor term $\boldsymbol{\sigma}$ is inserted into the equilibrium relationship (A.13). This procedure yields an expression depending exclusively on the displacement ansatz and on the material stiffness:

$$(k^2\,\boldsymbol{\Gamma} - \rho\,\omega^2\,\mathbf{1}) \cdot \mathbf{A}_0 = 0 \qquad \text{with} \qquad \boldsymbol{\Gamma} = \mathbf{C} \cdot \mathbf{n} \cdot \mathbf{n}, \tag{A.19}$$

where $\boldsymbol{\Gamma}$ denotes the acoustic tensor and $\mathbf{1}$ denotes the second-order identity tensor. Dividing (A.19) by k^2, specifying the resulting expression for k according to (A.16) as well as

for ω according to (A.14), and considering the expression for the wave propagation speed according to (A.15), leads to the following eigenvalue problem

$$\left[\mathbf{\Gamma} - \rho \left(\frac{\omega}{k}\right)^2 \mathbf{1}\right] \cdot \mathbf{A}_0 = 0 \;\Rightarrow\; \left[\mathbf{\Gamma} - \rho \left(\frac{2\,\pi\,f}{\frac{2\,\pi}{\lambda}}\right)^2 \mathbf{1}\right] \cdot \mathbf{A}_0 = 0 \;\Rightarrow\; \left[\mathbf{\Gamma} - \rho\,v^2\,\mathbf{1}\right] \cdot \mathbf{A}_0 = 0\,. \quad \text{(A.20)}$$

The relevant non-trivial solution of (A.20) exhibits $\mathbf{A}_0 \neq 0$, where $\mathbf{A}_0$ is the eigenvector. The corresponding eigenvalue is the wave propagation speed. As to allow for a non-trivial solution, the wave propagation speed v must be related to the stiffness of the material, such that the term within the brackets in (A.20) is equal to zero. This procedure is detailed in the following, by means of two examples.

Example 1: longitudinal wave propagation

The direction of particle vibration and the direction of wave propagation are aligned in case of a longitudinal wave. In other words, the movement of the medium points in the same direction or in the opposite direction compared with the propagation direction of the wave. If this propagation coincides with the x_1-axis of a Cartesian coordinate system, the amplitude vector and the wave vector can be expressed as

$$\mathbf{A}_0 = \begin{bmatrix} A_1 \\ 0 \\ 0 \end{bmatrix}, \qquad \mathbf{k} = \begin{bmatrix} k \\ 0 \\ 0 \end{bmatrix}. \quad \text{(A.21)}$$

Insertion of (A.21) into the displacement ansatz (A.17) yields the following expressions for the displacement components,

$$u_1(\mathbf{x}, t) = A_1\,\cos(k\,x_1 - \omega\,t)\,, \qquad u_2(\mathbf{x}, t) = u_3(\mathbf{x}, t) = 0\,. \quad \text{(A.22)}$$

Equations (A.22) illustrate that no displacements occur along the x_2- and x_3-directions. Moreover the displacements along the x_1-direction only depend on the x_1-coordinate and on the time t. Computation of the linearized strain tensor components based on (A.22) yields:

$$\varepsilon_{11} = \frac{\partial u_1}{\partial x_1} = -k\,A_1\,\sin(k\,x_1 - \omega\,t) \qquad \varepsilon_{12} = \frac{1}{2}\left(\frac{\partial u_1}{\partial x_2} + \frac{\partial u_2}{\partial x_1}\right) = 0 \qquad \varepsilon_{13} = \frac{1}{2}\left(\frac{\partial u_1}{\partial x_3} + \frac{\partial u_3}{\partial x_1}\right) = 0$$

$$\varepsilon_{21} = \frac{1}{2}\left(\frac{\partial u_2}{\partial x_1} + \frac{\partial u_1}{\partial x_2}\right) = 0 \qquad \varepsilon_{22} = \frac{\partial u_2}{\partial x_2} = 0 \qquad \varepsilon_{23} = \frac{1}{2}\left(\frac{\partial u_2}{\partial x_3} + \frac{\partial u_3}{\partial x_2}\right) = 0$$

$$\varepsilon_{31} = \frac{1}{2}\left(\frac{\partial u_3}{\partial x_1} + \frac{\partial u_1}{\partial x_3}\right) = 0 \qquad \varepsilon_{32} = \frac{1}{2}\left(\frac{\partial u_3}{\partial x_2} + \frac{\partial u_2}{\partial x_3}\right) = 0 \qquad \varepsilon_{33} = \frac{\partial u_3}{\partial x_3} = 0\,.$$

$$\text{(A.23)}$$

Equation (A.23) describes a uniaxial strain state (i.e. just one component differs from zero). Insertion of the strain state (A.23) into the generalized Hooke's law,

$$
\begin{bmatrix}
\sigma_{11} \\
\sigma_{22} \\
\sigma_{33} \\
\sqrt{2}\,\sigma_{23} \\
\sqrt{2}\,\sigma_{13} \\
\sqrt{2}\,\sigma_{12}
\end{bmatrix}
=
\begin{bmatrix}
C_{1111} & C_{1122} & C_{1133} & 0 & 0 & 0 \\
C_{2211} & C_{2222} & C_{2233} & 0 & 0 & 0 \\
C_{3311} & C_{3322} & C_{3333} & 0 & 0 & 0 \\
0 & 0 & 0 & 2\,C_{2323} & 0 & 0 \\
0 & 0 & 0 & 0 & 2\,C_{1313} & 0 \\
0 & 0 & 0 & 0 & 0 & 2\,C_{1212}
\end{bmatrix}
\begin{bmatrix}
\varepsilon_{11} \\
\varepsilon_{22} \\
\varepsilon_{33} \\
\sqrt{2}\,\varepsilon_{23} \\
\sqrt{2}\,\varepsilon_{13} \\
\sqrt{2}\,\varepsilon_{12}
\end{bmatrix}
\quad
\begin{array}{l}
\text{considering} \\
\text{symmetries:} \\[4pt]
C_{2211} = C_{1122} \\
C_{3311} = C_{1133} \\
C_{3322} = C_{2233}\,,
\end{array}
$$

$$\tag{A.24}$$

leads to a triaxial stress state fluctuating along the x_1-axis (i.e. it is one-dimensional):

$$
\sigma_{11} = C_{1111}\Big[-k\,A_1\,\sin(k\,x_1 - \omega\,t)\Big] \qquad\qquad \sigma_{12} = 0 \qquad\qquad \sigma_{13} = 0
$$

$$
\sigma_{21} = 0 \qquad\qquad \sigma_{22} = C_{1122}\Big[-k\,A_1\,\sin(k\,x_1 - \omega\,t)\Big] \qquad\qquad \sigma_{23} = 0 \tag{A.25}
$$

$$
\sigma_{31} = 0 \qquad\qquad \sigma_{32} = 0 \qquad\qquad \sigma_{33} = C_{1133}\Big[-k\,A_1\,\sin(k\,x_1 - \omega\,t)\Big]\,.
$$

Inserting of (A.25) together with the displacement ansatz (A.22) into the equilibrium conditions (A.13) yields

$$
\frac{\partial\sigma_{11}}{\partial x_1} + \frac{\partial\sigma_{21}}{\partial x_2} + \frac{\partial\sigma_{31}}{\partial x_3} = \rho\,\frac{\partial^2 u_1}{\partial t^2} \quad\Rightarrow\quad C_{1111}\Big[-k^2\,A_1\,\cos(k\,x_1 - \omega\,t)\Big] = -\rho\,\omega^2\,A_1\,\cos(k\,x_1 - \omega\,t)
$$

$$
\frac{\partial\sigma_{12}}{\partial x_1} + \frac{\partial\sigma_{22}}{\partial x_2} + \frac{\partial\sigma_{32}}{\partial x_3} = \rho\,\frac{\partial^2 u_2}{\partial t^2} \quad\Rightarrow\quad 0 = 0 \tag{A.26}
$$

$$
\frac{\partial\sigma_{13}}{\partial x_1} + \frac{\partial\sigma_{23}}{\partial x_2} + \frac{\partial\sigma_{33}}{\partial x_3} = \rho\,\frac{\partial^2 u_3}{\partial t^2} \quad\Rightarrow\quad 0 = 0
$$

The second and the third line of (A.26) illustrate that the equilibrium is fulfilled trivially in the x_2- and x_3-directions. Dividing the non-trivial equilibrium condition in the x_1-direction by $-k^2$ leads to

$$
\left[C_{1111} - \rho\left(\frac{\omega}{k}\right)^2\right] A_1\,\cos(k\,x_1 - \omega\,t) = 0\,. \tag{A.27}
$$

Specifying (A.27) for ω according to (A.14) and for k according to (A.16), and considering the expression for the wave propagation speed v according to (A.15) yields:

$$
\big[C_{1111} - \rho\,v_l^2\big] A_1\,\cos(k\,x_1 - \omega\,t) = 0\,, \tag{A.28}
$$

where v_l is the propagation speed of the analyzed longitudinal wave. For a non-trivial solution of (A.28), the expression within in the squared brackets has to vanish:

$$
C_{1111} - \rho\,v_l^2 = 0 \quad\Rightarrow\quad v_l = \sqrt{\frac{C_{1111}}{\rho}}\,. \tag{A.29}
$$

Equation (A.29) illustrates that the propagation speed of a longitudinal wave increases with increasing stiffness and with decreasing mass density of the material.

Example 2: shear wave propagation

Shear or transverse waves relate to particle motion directions being perpendicular to the direction of wave propagation. In a Cartesian coordinate system, we let the propagation direction and the particle vibration direction correspond to the x_1-axis and the x_2-axis, respectively. This allows us to express the amplitude vector and the wave vector as

$$\mathbf{A}_0 = \begin{bmatrix} 0 \\ A_2 \\ 0 \end{bmatrix}, \qquad \mathbf{k} = \begin{bmatrix} k \\ 0 \\ 0 \end{bmatrix}. \tag{A.30}$$

Insertion of (A.30) into the displacement ansatz (A.17) yields the following expressions for the displacement components

$$u_1(\mathbf{x}, t) = 0 \qquad u_2(\mathbf{x}, t) = A_2 \cos(k\, x_1 - \omega\, t) \qquad u_3(\mathbf{x}, t) = 0. \tag{A.31}$$

Equations (A.31) illustrate, that no displacements occur along the x_1- and x_3-directions. Moreover the displacements in the x_2-direction only depend on the x_1-coordinate and on the time t. Computation of the linearized strain tensor components based on (A.31) yields:

$$\varepsilon_{11} = \frac{\partial u_1}{\partial x_1} = 0 \qquad \varepsilon_{12} = \frac{1}{2}\left(\frac{\partial u_1}{\partial x_2} + \frac{\partial u_2}{\partial x_1}\right) = -\frac{k\,A_2}{2}\sin(k\,x_1 - \omega\,t) \qquad \varepsilon_{13} = \frac{1}{2}\left(\frac{\partial u_1}{\partial x_3} + \frac{\partial u_3}{\partial x_1}\right) = 0$$

$$\varepsilon_{21} = \frac{1}{2}\left(\frac{\partial u_2}{\partial x_1} + \frac{\partial u_1}{\partial x_2}\right) = -\frac{k\,A_2}{2}\sin(k\,x_1 - \omega\,t) \qquad \varepsilon_{22} = \frac{\partial u_2}{\partial x_2} = 0 \qquad \varepsilon_{23} = \frac{1}{2}\left(\frac{\partial u_2}{\partial x_3} + \frac{\partial u_3}{\partial x_2}\right) = 0$$

$$\varepsilon_{31} = \frac{1}{2}\left(\frac{\partial u_3}{\partial x_1} + \frac{\partial u_1}{\partial x_3}\right) = 0 \qquad \varepsilon_{32} = \frac{1}{2}\left(\frac{\partial u_3}{\partial x_2} + \frac{\partial u_2}{\partial x_3}\right) = 0 \qquad \varepsilon_{33} = \frac{\partial u_3}{\partial x_3} = 0. \tag{A.32}$$

Equations (A.32) describe a two-axial strain state in the x_1-x_2-plane (a pure shear strain state). Inserting the strain state (A.32) into the generalized Hooke's law, leads to a pure shear stress state in the x_1-x_2-plane, fluctuating along the x_1-axis:

$$\sigma_{11} = 0 \qquad\qquad \sigma_{12} = C_{1212}\left[-\frac{k\,A_2}{2}\sin(k\,x_1 - \omega\,t)\right] \qquad \sigma_{13} = 0$$

$$\sigma_{21} = C_{1212}\left[-\frac{k\,A_2}{2}\sin(k\,x_1 - \omega\,t)\right] \qquad \sigma_{22} = 0 \qquad\qquad \sigma_{23} = 0$$

$$\sigma_{31} = 0 \qquad\qquad \sigma_{32} = 0 \qquad\qquad \sigma_{33} = 0. \tag{A.33}$$

Insertion of (A.33) together with the displacement ansatz (A.31) into the equilibrium condition (A.13) yields

$$
\frac{\partial \sigma_{11}}{\partial x_1} + \frac{\partial \sigma_{21}}{\partial x_2} + \frac{\partial \sigma_{31}}{\partial x_3} = \rho \frac{\partial^2 u_1}{\partial t^2} \quad \Rightarrow \quad 0 = 0
$$

$$
\frac{\partial \sigma_{12}}{\partial x_1} + \frac{\partial \sigma_{22}}{\partial x_2} + \frac{\partial \sigma_{32}}{\partial x_3} = \rho \frac{\partial^2 u_2}{\partial t^2} \quad \Rightarrow \quad C_{1212}\left[-\frac{k^2 A_2}{2} \cos(k\, x_1 - \omega\, t) \right] = -\frac{\rho\, \omega^2 A_2}{2} \cos(k\, x_1 - \omega\, t)
$$

$$
\frac{\partial \sigma_{13}}{\partial x_1} + \frac{\partial \sigma_{23}}{\partial x_2} + \frac{\partial \sigma_{33}}{\partial x_3} = \rho \frac{\partial^2 u_3}{\partial t^2} \quad \Rightarrow \quad 0 = 0
$$

$$\text{(A.34)}$$

The first and the third line in (A.34) illustrate that equilibrium is fulfilled trivially in the x_1- and x_3-directions. Dividing the non-trivial equilibrium condition in the x_2-direction by $-k^2$ leads to

$$
\left[C_{1212} - \rho \left(\frac{\omega}{k} \right)^2 \right] \frac{A_2}{2} \cos(k\, x_1 - \omega\, t) = 0 \, . \tag{A.35}
$$

Insertion of ω according to (A.14) and of k according to (A.16) into the quotient ω/k of (A.35), and considering the wave propagation speed v according to (A.15) yields

$$
\left[C_{1212} - \rho\, v_t^2 \right] \frac{A_2}{2} \cos(k\, x_1 - \omega\, t) = 0 \, , \tag{A.36}
$$

where v_t is the propagation speed of the analyzed shear wave. For a non-trivial solution of (A.36) the expression within the squared brackets has to vanish:

$$
C_{1212} - \rho\, v_t^2 = 0 \quad \Rightarrow \quad v_t = \sqrt{\frac{C_{1212}}{\rho}} \, . \tag{A.37}
$$

Equation (A.37) illustrates that the propagation speed of a shear wave increases with increasing stiffness and with decreasing mass density.

A.2.4 Isotropic, linear elastic materials

The stiffness of isotropic, linear elastic materials is characterized by two independent material constants. The speeds of longitudinal waves and shear waves allow for identifying two independent material constants and, therefore, for a complete stiffness characterization of an isotropic, elastic material. In other words, Young's modulus E, Poisson's ratio ν, bulk modulus K, shear modulus G, and Lamé's constant λ can be computed, according to

(A.29) and (A.37), as

$$
\begin{aligned}
E &= \frac{C_{1212}\left(3\,C_{1111} - 4\,C_{1212}\right)}{C_{1111} - C_{1212}} & \Rightarrow \qquad E &= \frac{\rho\,v_t^2\left(3\,v_l^2 - 4\,v_t^2\right)}{v_l^2 - v_t^2} \\[2ex]
\nu &= \frac{C_{1111} - 2\,C_{1212}}{2\left(C_{1111} - C_{1212}\right)} & \Rightarrow \qquad \nu &= \frac{v_l^2 - 2\,v_t^2}{2\left(v_l^2 - v_t^2\right)} \\[2ex]
K &= C_{1111} - \frac{4}{3}\,C_{1212} & \Rightarrow \qquad K &= \frac{\rho}{3}\left(3\,v_l^2 - 4\,v_t^2\right) \\[2ex]
G &= C_{1212} & \Rightarrow \qquad G &= \rho\,v_t^2 \\[2ex]
\lambda &= C_{1111} - 2\,C_{1212} & \Rightarrow \qquad \lambda &= \rho\left(v_l^2 - 2\,v_t^2\right)
\end{aligned}
\tag{A.38}
$$

Appendix B

Practical line of actions for performing of mechanical unloading and ultrasonics testing

B.1 Casting of specimens

The specimen casting process consists of several steps, which are described below. First, the cementitious raw materials are weighted with a precision up to $\pm 0.005\,\mathrm{g}$ and put into a mixing bowl. If fly ash is used as a supplementary cementitious material, the required mass is added and both materials are well mixed by hand using a metal blunger, until a satisfactory dispersion level is reached, related to a quasi-homogeneous colour of the mixed powder. Water is weighted with the same precision and added. From this time instant, the age of the subsequently produced samples is recorded.

Materials are then mixed, in the mixing bowl, using a metal blunger mounted to an electrical screw driver, that is capable of mixing using two different rotation speeds. During the first 30 seconds, we use the lower mixing speed, in order to prevent excessive dust creation. This is followed by increasing the mixing speed to the maximum possible level and continuous mixing for another 30 seconds. After one minute of continuous mixing, we stop and manually remove any unmixed clusters of dry cementitious powder from the bottom and the lateral surfaces of the mixing bowl. This action takes another minute, i.e. up to two minutes since the beginning of mixing. Then, the mixing of the fresh paste is started again, this time using only the highest speed level, for additional 60 seconds, finishing exactly after 3 minutes after the initial contact between water and the cementitious materials.

Casting into the mold is the next crucial step leading to homogeneous specimens without any bubbles of entrapped air. We place the empty mold on a vibrating table and incline it, such that the angle between the longitudinal axis of the mold and the horizontal plane of the vibrating table amounts to approximately 30 °. Next, we slowly fill the inclined mold by means of sliding the fresh paste first through a funnel and then along the inner surface of the inclined mold rather than letting it simply fall down into the mold. This method reduces the risk of segregation of fine particles and air entrapment to a very satisfactory minimum. During the filling procedure, the mold is constantly vibrated in order to get air bubbles to the top of the mold. After the filling process, we remove excessive paste from the top surface of the plastic mold, place a rubber ring around the filling hole, and seal the filling hole using a transparent circular plastic plate which is fixed to the top surface of the mold by means of three screws, until the rubber ring is visually compressed. This ring ensures an air-proof sealing of the sample, and it provides the possibility to remove excessive paste once the ring is removed during demolding.

Filled molds are finally stored in a climate chamber conditioned to 20 degrees centigrade and to 90 % relative air humidity. After 24 hours of curing, samples are demolded and prepared for testing. In order to facilitate demolding, we use specially designed and custom-made formworks, made from a non-absorbent and scratch-resistant hard plastic. The formworks consist of two parts, held together by a lower platform, into which both parts slide in, and two metal tightening collars. The top surface of the mold contains holes for screws pushing the aforementioned plastic cover against the rubber ring. Prior to the mold-filling process, we apply a thin layer of water-resistant synthetic grease on the inner walls and the bottom of the mold, which ensures simple demolding of the sample without applying notable forces on the very fragile specimen. In order to achieve the desired co-planarity of top and bottom surfaces, we carefully scratch the top of the specimen with a Stanley knife, using the top of the mold surface as a guide. Should the sample contain any large bubbles of entrapped air, in the vicinity of the top or bottom of the specimen, we cut away the affected region of the specimen, followed by Stanley knife shaving. This ensures a well prepared specimen for testing either by means of mechanical unloading or by means of ultrasonics testing.

B.2   Practical steps for mechanical unloading testing

We characterize the stiffness of cement pastes by means of quantifying the unloading modulus. In order to apply, as central as possible, normal forces during stiffness testing, we first attach (using Scotch tape) a pair of steel cylinders with bottlenecks, in a serial ar-

rangement, to the specimen, see Fig. B.1. Then we cover the specimen with a plastic food preservation foil in order to reduce evaporation of free (i.e. unbound) water from the otherwise uncovered surface of the specimen.
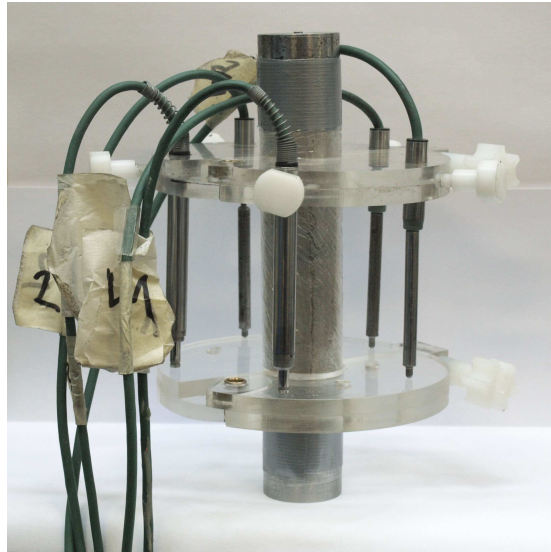
Figure B.1: Test setup consisting of two metal cylinders with bottlenecks, attached to the cylindrical specimen using a Scotch tape, and two plexiglass rings holding five LVDTs which are evenly distributed around the perimeter of the specimen

For the strain quantification, we used the following setup: to obtain over-determined measurements of sample deformations during loading and unloading, we use five independent LVDTs instead of the minimum three, evenly spaced with an angular distance of $72°$ around the central axis of the specimen. All five LVDTs measure the relative displacement of the two plexiglass rings that are clamped to the specimen at predefined locations, see Fig. B.1. This way, the plexiglass rings are in continuous contact around the perimeter of the sample. We mount both plexiglass rings in a distance from the end of the specimen, which amounts to the one times the cylinder diameter (i.e. 30 mm), to minimize the impact of the inevitable self-equilibrated shear forces within the interfaces between the sample and the adjacent metal cylinders. This distance is achieved with the help of three distance pieces used to keep the plexiglass rings in position during clamping.

The mean value of the five LVDT measurements together with the distance of the plexiglass rings allows for the calculation of normal strains in loading direction. Individual displacement fluctuations around the mean value, in turn, are related to bending, resulting mainly from load eccentricity, see Section B.2.1.

B.2.1   Calculation of the effective eccentricity during mechanical unloading testing

We combine our deformation measurements with first-order beam theory, i. e. the specimen part between the two plexiglass rings is idealized as a simply supported beam with axial coordinate x. The beam is loaded, at both ends, by a compressive normal force P exhibiting an eccentricity e in the negative z-direction. Therefore, both the normal force N and the bending moment M are constant along the beam

$$N(x) = -P, \qquad M(x) = P\,e. \tag{B.1}$$

Axial displacements due to normal force and bending moment

The normal stress σ resulting from a normal force N can be described as

$$\sigma = \frac{N}{A} = -\frac{P}{A}. \tag{B.2}$$

Considering Hooke's law and (B.2), the strain in x-direction is defined as

$$\varepsilon_{xx} = \frac{\sigma}{E} = -\frac{P}{EA} = \frac{du}{dx}, \tag{B.3}$$

where $\frac{du}{dx}$ is the derivation of the displacement component u in x-direction. Integration of (B.3) yields the displacement field

$$u(x) = -\frac{P\,x}{EA} + u(x=0), \tag{B.4}$$

where $u(x=0)$ is the displacement at the beginning of the beam. It is considered to be equal to zero:

$$u(x=0) = 0. \tag{B.5}$$

Specifying (B.4) for the beam length l_m allows for calculating the displacement at the end of the beam

$$u(x=l_m) = -\frac{P\,l_m}{EA}. \tag{B.6}$$

Knowledge of the bending moment $M(x)$ and the bending stiffness EI allows for determination of the angle of cross sectional rotation φ:

$$\frac{d\varphi(x)}{dx} = -\frac{M(x)}{EI}. \tag{B.7}$$

Insertion of the expression for the moment (B.1) into (B.7) and integration yields

$$\varphi(x) = -\frac{P\,e}{EI}\,x + \varphi(x=0). \tag{B.8}$$

Considering the symmetry condition in the middle of the beam $(x = \frac{l_m}{2})$

$$\varphi\left(x = \frac{l_m}{2}\right) = 0 \tag{B.9}$$

and specifying (B.8) for $(x = \frac{l_m}{2})$ yields

$$\varphi\left(x = \frac{l_m}{2}\right) = -\frac{P\,e}{EI}\frac{l_m}{2} + \varphi(x = 0) = 0. \tag{B.10}$$

Solving for $\varphi(x = 0)$ delivers

$$\varphi(x = 0) = \frac{P\,e\,l_m}{2\,EI}. \tag{B.11}$$

Insertion of (B.11) into (B.8) yields

$$\varphi(x) = \frac{P\,e\,l_m}{2\,EI} - \frac{P\,e}{EI}\,x. \tag{B.12}$$

The axial displacement $u(x, z)$ that results from the bending moment reads as

$$u(x, z) = -\varphi(x)\,z. \tag{B.13}$$

Insertion of (B.12) into (B.13) yields the bending-induced displacements in x-direction as

$$u(x, z) = -\left[\frac{P\,e}{EI}\left(\frac{l_m}{2} - x\right)\right]z. \tag{B.14}$$

Combining (B.4) and (B.14) yields the total axial displacement field

$$u_{tot}(x, z) = -\frac{P\,x}{EA} - \frac{P\,e}{EI}\left(\frac{l_m}{2} - x\right)z. \tag{B.15}$$

Subtraction of the displacement at the end from the displacement at the beginning of the beam, leads to the following beam-theory-analogon to the LVDT measurements

$$u_{tot}(x = 0) - u_{tot}(x = l_m) = \Delta u_{tot} =$$
$$-\frac{P\,e}{EI}\frac{l_m}{2}z - \left[-\frac{P\,l_m}{EA} - \frac{P\,e}{EI}\left(\frac{l_m}{2} - l_m\right)z\right] + \frac{P\,l_m}{EA} - \frac{P\,e}{EI}l_m\,z$$
$$= \frac{P\,l_m}{E}\cdot\left(\frac{1}{A} - \frac{e}{I}z\right) = \frac{P\,l_m}{EA}\left(1 - \frac{e\,z}{i^2}\right) \tag{B.16}$$

where e is the eccentricity of the acting normal force and the moment of inertia I is

$$I = A\,i^2 \tag{B.17}$$

with i as the radius of inertia.

Measurements of the LVDTs and calculation of the eccentricity

Let $\phi_1, \phi_2, \phi_3, \phi_4$ and ϕ_5 denote the position angles of the five LVDTs with respect to the z-axis. Considering that ϕ_1 will be identified, allows for the determination of the other four LVDT angles as:

$$\phi_2 = \phi_1 + \frac{2\pi}{5}$$
$$\phi_3 = \phi_1 + \frac{4\pi}{5}$$
$$\phi_4 = \phi_1 + \frac{6\pi}{5}$$
$$\phi_5 = \phi_1 + \frac{8\pi}{5}. \tag{B.18}$$

Specifying (B.16) for

$$z_1 = r_w \cos(\phi_1), \tag{B.19}$$

allows for calculating the relative displacements of the first LVDT

$$\Delta u_{tot}(\phi_1) = \frac{P\,l_m}{EA}\left(1 - \frac{e\,z_1}{i^2}\right) = \frac{P\,l_m}{EA}\left(1 - \frac{e\,r_w}{i^2}\cos(\phi_1)\right), \tag{B.20}$$

and of the second LVDT as

$$\Delta u_{tot}(\phi_2) = \frac{P\,l_m}{EA}\left[1 - \frac{e\,r_w}{i^2}\cos\left(\phi_1 + \frac{2\pi}{5}\right)\right]. \tag{B.21}$$

The relative displacements of the other three LVDTs can be calculated, based on (B.18), by analogy to (B.20) and (B.21).

The measured displacements of the LVDTs (Δu_{tot}^{exp}) are now compared with their modeling counterparts (Δu_{tot}^{mod}). For the first LVDT, we write formally

$$\Delta u_{tot}^{exp}(\phi_1) \quad \leftrightarrow \quad \Delta u_{tot}^{mod}(\phi_1) = \frac{P\,l_m}{EA}\left(1 - \frac{e\,r_w}{i^2}\cos(\phi_1)\right). \tag{B.22}$$

Generalizing (B.22) yields for the j-th LVDT:

$$\Delta u_{tot}^{exp}(\phi_j) \quad \leftrightarrow \quad \Delta u_{tot}^{mod}(\phi_j) = \frac{P\,l_m}{EA}\left[1 - \frac{e\,r_w}{i^2}\cos\left(\phi_1 + \frac{(j-1)\,2\pi}{5}\right)\right]. \tag{B.23}$$

The difference between measured displacements and modeled displacements depends on e and ϕ_1. This error

$$Error(e, \phi_1) = \sum_{j=1}^{5}\left(\Delta u_{tot}^{exp}(\phi_j) - \Delta u_{tot}^{mod}(\phi_j)\right)^2 \tag{B.24}$$

reaches a minimum for e and ϕ_1 satisfying

$$\frac{\delta Error}{\delta e} = 0, \qquad \frac{\delta Error}{\delta \phi_1} = 0. \tag{B.25}$$

The eccentricity can finally be identified from deriving (B.25) with respect to e

$$
\frac{\delta Error}{\delta e} =
$$
$$
\sum_{j=1}^{5} 2 \left(\Delta u_{tot}^{exp}(\phi_j) - \Delta u_{tot}^{mod}(\phi_j) \right) \left[\frac{P\, l_m}{EA} \frac{r_w}{i^2} \cos\left(\phi_1 + \frac{(j-1)\,2\pi}{5} \right) \right] = 0,
$$

$$(B.26)$$

and with respect to ϕ_1

$$
\frac{\delta Error}{\delta \phi_1} =
$$
$$
\sum_{j=1}^{5} 2 \left(\Delta u_{tot}^{exp}(\phi_j) - \Delta u_{tot}^{mod}(\phi_j) \right) \frac{P\, l_m}{EA} \frac{e\, r_w}{i^2} \left[-\sin\left(\phi_1 + \frac{(j-1)\,2\pi}{5} \right) \right] = 0.
$$

$$(B.27)$$

From solving the system of equations (B.26) and (B.27), the eccentricity e and the position angle ϕ_1 can be identified.

B.3 Practical steps for ultrasonics testing

We used ultrasonic wave speeds for determination of the stiffness of a sample. For this task we employed a 600 MHz, 10 GS/s (gigasamples per second) dual-channel, digital oscilloscope form LeCroy, waveRunner 62Xi together with ultrasonic transversal transducers from Parametrics, NDT V150-RB with a frequency of 250 kHz.

To measure the stiffness using ultrasonics testing, we position the sample in between two transducers, which are held in position by a stiff steel frame. This frame ensures a serial arrangement as well as a good contact between all the components. One of the transducers (emitter) sends a transversal wave with a specific frequency. The wave is traveling through the sample and it is recorded by the other transducer (receiver).

The emitter sends a shear wave with a specific frequency through the sample, but due to inevitable inaccuracies, also a small longitudinal wave signal is produced. Interestingly, this allows also for determination of the longitudinal wave speed, as described next. The oscilloscope displays the received wave signal as a function of time. The first signal arriving at the receiver stems from the longitudinal wave. Its arrival at the receiver can be easily identified as the first fluctuation deviating from the initial flat line. Once the signal starts to increase rapidly by an order of magnitude, the transversal wave has arrived at the receiver. As a rule of thumb, the transversal signal needs two times longer than the longitudinal signal.

Figure B.2: Test setup consisting of the cylindrical cement specimen, the steel frame and the transducers covered by thin honey layers and food preservation foils

Before the start of ultrasonics measurements, we prepare the transducers in the following way: directly on the transducer surfaces we apply a thin layer of honey and cover it with a plastic food preservation foil, in order to create a viscous layer that ensures a good contact of the sample with the transducer. Since the honey layer and the plastic film have a non-zero thickness, we measured the travel time of ultrasonic waves through two layers of honey and two plastic foils without any sample, resulting in a reference runtime t_{ref}. Subsequently, the samples were investigated by putting them between the transducers (Fig. B.2), resulting in total signal runtimes t_{tot}, through the sample plus the two layers of honey and the two food preserving foils, see Fig. B.2. Hence, the travel time of waves only through the sample is

$$t_{sample} = t_{tot} - t_{ref}. \tag{B.28}$$

Finally, t_{sample} and the sample height h_{sample} allow for the identification of the sought wave speed:

$$v_{wave} = \frac{h_{sample}}{t_{sample}}. \tag{B.29}$$

Applying axial compressive loading to the setup, using a metal load plate, improves the intensity of the observed waves but care has to be taken that the sample is not damaged.

Appendix C

Calorimetry testing

A differential calorimeter, ToniCal Trio type 7339, was used. The calorimeter hosts three measuring cells, such that three independent tests can be carried out simultaneously, see Fig. C.1.

Figure C.1: Top view onto calorimeter ToniCal Trio type 7339 with three independent measuring cells

The measurement principle is briefly described next. During a test, every cell hosts one reference sample and one measurement sample, whereby both samples are kept in separated test tubes. The calorimeter measures the difference of the heat release rates between the test sample and the reference sample, by quantifying the energy needed to keep the measuring cells and the samples at a constant test temperature T_{in}. To this end,

the temperature of the ambient air around the calorimeter, T_{ex}, has to be as constant as possible, and by a minimum of three degrees Celsius smaller than the test temperature:

$$T_{in} - T_{ex} \geq 3\,°\text{C}. \tag{C.1}$$

The steady state heat loss through the isolated walls of the calorimeter requires a constant heating of the measuring cells, even if the samples are inert (i.e. even if samples neither generate nor consume energy). Once energy is released from the test sample, e.g. by the hydration reaction of cement and water, the heating of the measuring cell can be reduced accordingly and this opens the door to quantifying the heat release rate.

C.1 Testing equipment and sample preparation

The tests described herein, were carried out at a testing temperature amounting to

$$T_{in} = 20\,°\text{C}. \tag{C.2}$$

The ambient air was conditioned to a temperature of

$$T_{ex} = 16.7 \pm 0.2\,°\text{C}. \tag{C.3}$$

The satisfactory stable value of the ambient air temperature was accomplished by using an electrical oven to heat the room and, at the same time, by using an air conditioning system to cool the room. This rather energy consuming strategy resulted in almost stationary conditions throughout the tests. In order to buffer possible temperature fluctuations stemming from (forced) convection either from the oven or from the air conditioning system, the calorimeter was put into a box made from heat isolating boards (Fig. C.1). Notably, this box was open (and not sealed) in order to ensure that the calorimeter was surrounded by air with a temperature T_{ex} satisfying (C.1).

Three test series were carried out with three different cementitious paste samples, referring to the same initial water-to-cement mass ratios w/c and water-to-solid mass ratios w/s, as for mechanical unloading and ultrasonic testing:

- Paste 1: $w/c = w/s = 0.50$

- Paste 2: $w/c = w/s = 0.42$

- Paste 3: $w/c = 0.50$ and $w/s = 0.42$, i.e. the mass of solid binder is composed of 16 % fly ash and of 84 % cement

For calorimetry testing one reference sample and one test sample are inserted in a measuring cell, as described previously. The sample preparation is described in the following.

C.1.1   Reference sample preparation

As the reference sample for a test serves a well-cured and, therefore, quasi-inert sample. Its preparation is described next. For tests with paste 1 or 2 a test tube is filled with 10.0 ± 0.0005 g cement powder. For tests with paste 3 the 10.0 ± 0.0005 g of solid binder (exhibiting the desired dosages: 16 % fly ash and of 84 % cement) is premixed inside a small basin until a satisfactory dispersion is reached, before filling the cementitious powder into the test tube. The solid binders are compacted such that the filling level is equal to 56 mm, i.e. equal to the height of the filling block provided by Toni Technik. Compaction is carried out by lifting the test tube some millimeters out of the filling block and by letting it fall back to the bottom. The required water mass is added with a syringe in the next step. In order to comply with the desired initial water-to-solid mass ratio w/s, the water mass amounts to $w/s \cdot 10$ g, i.e. in case of paste 1, the desired water mass amounts to 5.0 g; in case of paste 2, the desired water mass amounts to 4.2 g; in case of paste 3, the desired water mass amounts to 4.2 g. A plastic paddle is used to mix the material and is left in the fresh cementitious paste after mixing. After that, the rod of the paddle is cut such that the test tube could be sealed by means of a food preserving foil (avoiding water evaporation). Then, the sample is stored in a climate chamber conditioned at $20\,°C$ (and 95 % relative air humidity). After more than one month of this heat treatment, the reference sample is taken out of the climate chamber, cooled to room temperature, and then inserted into the calorimeter.

C.1.2   Test sample preparation

As a test sample basically serves a freshly mixed cementitious paste. In contrast to the reference sample, distilled water and solid binders, are inserted *separately* into the calorimeter, i.e. they are not mixed before a stationary temperature regime is reached inside the sealed measuring cell. For the test sample preparation a plastic paddle is put headlong into a test tube. After that, 10 ± 0.0005 g binder are put into the same test tube and compacted in the same way as described for the reference sample. The required water mass, $w/s \cdot 10\,\text{g} + 0.25\,\text{g} \pm 0.0005\,\text{g}$ of distilled water is filled into a syringe by drawing back the plunger, but is not added to the solid constituents yet. Additional 0.25 g distilled water are added, in order to compensate the water loss inside the injection module, during the injection process. The test tube (containing both the compacted cementitious powder and the plastic paddle) and the syringe are inserted into the measuring cell of the calorimeter. The testing procedure is started subsequently, explained in Section C.2.

C.2 Testing procedure

After inserting the reference sample and the test sample into the calorimeter, each cell is sealed using a cover containing drill-holes, and is then conditioned to the test temperature of 20 °C. Once a stationary temperature regime is reached, the cementitious powder and water of the test sample are mixed without re-opening the calorimeter. To this end, an injection module is used that allows for mixing (from outside of the calorimeter) the cementitious powder and water inside a test tube embedded in a measuring cell. The functionality of this injection module is briefly described in the following.

- The injection module is a box-shaped plastic body ($78\,\text{mm} \times 70\,\text{mm} \times 25\,\text{mm}$) which is positioned above the test sample. The plastic paddle that is embedded (from the very beginning of the test) headlong in the cementitious powder of the test sample, passes (via existing drill-holes) both through the injection module and through the cover of the measuring cell. Turning (from outside of the calorimeter) the plastic rod results in mixing the material inside the test tube.

- Distilled water is initially stored in a syringe which is put headlong into the injection module. The injection module ensures that the syringes plunger is positioned right beneath a vertically movable plastic piston which passes (also via an existing drill-hole) through the cover of the measuring cell. Pushing (again from outside of the calorimeter) this plastic piston downwards, pushes the plunger into the syringe, such that the water is injected.

- Notably, the axis of the syringe and the axis of the test tube are *not aligned* with one another. Water is not simply dropping vertically into the test tube, but it is transported via an existing tunnel system through the injection module to the test tube. As a result, typically $0.25\,\text{g}$ of water do not arrive in the test tube, but stay in the tunnel system. In order to ensure that the desired amount of water is injected to the cement, a by $0.25\,\text{g}$ increased water mass has to be filled into the syringe, as described in Section C.1.

Sealing of the measuring cell is followed by a waiting period of typically 8 hours which is required to achieve a stationary temperature regime inside the measuring cell. Then, the piston is pushed downwards such that the water is injected and by rotating the plastic paddle mixer solid constituents and water are well mixed during 90 seconds. At the end of the mixing process, the plastic paddle is put back to the initial position, i.e. it is pushed down such that the paddle head is again in contact with the bottom of the test tube.

Once a stationary regime is reached, the ToniCAL software is started, so that the heat release rate values are stored. The heat release rate values $\dot{Q}(t)$ are the actual measurement values and are converted into the evolution of the cumulative heat release $Q(t)$ by the ToniCAL software, based on a time-integration principle of $\dot{Q}(t)$.

Appendix D

Detailed compilation of experimental results

The results of mechanical unloading testing of samples with $w/s = w/c = 0.50$ are shown in Tables D.1 and D.2. The results of ultrasonics testing of samples with $w/s = w/c = 0.50$ are shown in Tables D.3 and D.4.

The results of mechanical unloading testing of samples with $w/s = w/c = 0.42$ are shown in Tables D.5 and D.6. The results of ultrasonics testing of samples with $w/s = w/c = 0.42$ are shown in Tables D.7 and D.8.

The results of mechanical unloading testing of samples with $w/s = 0.42$ and $w/c = 0.50$ are shown in Tables D.9 and D.10. The results of ultrasonics testing of samples with $w/s = 0.42$ and $w/c = 0.50$ are shown in Tables D.11 and D.12. In the following tables, dimensionless hydration degree is denoted as ξ.

Table D.1: Results from mechanical unloading tests on a cement paste sample with $w/s = w/c = 0.50$, produced on Oct 30, 2013, at 12h38; six orthogonal diameters were measured as 29.9, 29.9, 30.1, 30.1, 30.3 and 30.1 mm

test no	age [h]	unloading moduli [GPa]			unloading speed [kN/s]			number of data points			eccentricity [mm]	ξ [%]
1	22.35	4.69	4.67	4.69	1.05	1.07	1.07	14	14	14	0.055	34.5
2	23.35	4.96	4.96	4.89	1.08	1.07	1.08	14	14	14	0.094	35.6
3	24.35	5.21	5.19	5.20	1.09	1.07	1.07	14	14	14	0.081	36.6

Table D.1 – continued from previous page

test no	age [h]	unloading moduli [GPa]			unloading speed [kN/s]			number of data points			eccentricity [mm]	ξ [%]
4	25.35	5.36	5.47	5.48	1.07	1.07	1.07	14	14	14	0.12	37.6
5	26.35	5.64	5.67	5.67	1.07	1.08	1.06	13	13	14	0.11	38.5
6	27.35	5.86	5.95	5.89	1.07	1.06	1.06	14	14	14	0.096	39.4
7	28.35	6.03	6.12	6.04	1.08	1.07	1.09	14	13	14	0.085	40.2
8	29.35	6.25	6.30	6.19	1.06	1.07	1.07	13	14	13	0.10	41.0
9	30.35	6.42	6.41	6.42	1.09	1.08	1.08	14	14	14	0.074	41.7
10	31.35	6.53	6.56	6.52	1.08	1.08	1.08	14	14	14	0.14	42.4
11	32.35	6.64	6.78	6.78	1.08	1.08	1.06	14	14	14	0.15	43.0
12	33.35	6.94	6.83	6.89	1.07	1.08	1.09	14	14	14	0.13	43.7
13	34.35	7.05	6.99	7.03	1.05	1.07	1.08	14	14	14	0.10	44.3
14	35.35	7.12	7.20	7.09	1.07	1.06	1.09	15	14	14	0.12	44.9
15	36.35	7.24	7.35	7.15	1.09	1.05	1.07	14	14	14	0.13	45.4
16	37.35	7.40	7.28	7.36	1.08	1.06	1.08	14	14	14	0.12	46.0
17	38.35	7.48	7.47	7.50	1.09	1.09	1.09	13	14	14	0.089	46.5
18	39.35	7.53	7.47	7.60	1.07	1.08	1.09	14	13	14	0.15	47.0
19	40.35	7.61	7.76	7.66	1.06	1.07	1.07	14	14	14	0.11	47.5
20	41.35	7.78	7.81	7.77	1.02	1.09	1.08	13	13	14	0.16	48.0
21	42.35	7.89	7.83	7.82	1.06	1.10	1.08	14	14	14	0.099	48.5
22	43.35	8.04	7.99	8.04	1.07	1.08	1.09	14	14	14	0.086	48.9
23	44.35	8.10	8.10	8.02	1.08	1.06	1.08	13	14	14	0.074	49.4
24	45.35	7.94	8.09	8.14	1.07	1.06	1.07	14	13	14	0.17	49.8
25	46.35	8.09	8.10	8.09	1.08	1.06	1.08	14	13	14	0.15	50.2
26	48.28	8.46	8.48	8.60	1.08	1.08	1.08	14	13	14	0.17	51.0
27	49.28	8.66	8.54	8.64	1.09	1.09	1.09	14	14	14	0.16	51.3
28	50.28	8.58	8.71	8.62	1.09	1.09	1.08	14	13	14	0.12	51.7
29	51.28	8.75	8.77	8.75	1.10	1.08	1.08	13	14	14	0.20	52.1
30	52.28	8.82	8.54	8.75	1.07	1.07	1.09	13	14	13	0.17	52.4
31	53.28	8.78	8.78	8.73	1.09	1.09	1.09	14	13	13	0.17	52.7
32	54.28	8.85	9.03	8.94	1.10	1.09	1.07	13	14	14	0.17	53.0
33	55.28	9.24	9.07	8.91	1.09	1.10	1.08	14	14	14	0.12	53.3
34	56.28	9.15	8.97	9.08	1.09	1.09	1.06	14	14	14	0.18	53.6
35	57.28	9.02	9.07	9.03	1.09	1.09	1.07	14	13	14	0.18	53.9

Table D.1 – continued from previous page

test no	age [h]	unloading moduli [GPa]			unloading speed [kN/s]			number of data points			eccentricity [mm]	ξ [%]
36	58.28	8.93	9.14	9.19	1.09	1.09	1.09	13	14	13	0.19	54.2
37	59.28	9.21	9.22	9.19	1.08	1.10	1.09	14	13	14	0.13	54.5
38	60.28	9.42	9.23	9.42	1.09	1.09	1.08	14	13	13	0.15	54.7
39	61.28	9.19	9.27	9.23	1.08	1.09	1.10	13	14	13	0.20	55.0
40	62.28	9.36	9.32	9.30	1.09	1.09	1.07	13	14	14	0.19	55.2
41	63.28	9.45	9.30	9.40	1.07	1.09	1.08	13	14	13	0.14	55.5
42	64.28	9.42	9.62	9.34	1.07	1.09	1.10	13	14	13	0.19	55.7
43	65.28	9.78	9.56	9.38	1.10	1.09	1.08	13	14	13	0.15	55.9
44	66.28	9.40	9.39	9.44	1.09	1.10	1.10	13	13	13	0.19	56.1
45	67.28	9.42	9.53	9.59	1.09	1.09	1.09	13	13	13	0.15	56.3
46	68.28	9.70	9.54	9.52	1.11	1.10	1.09	14	14	13	0.17	56.5
47	69.28	9.46	9.58	9.59	1.10	1.09	1.10	13	14	14	0.16	56.7
48	70.28	9.68	9.62	9.86	1.08	1.09	1.10	14	14	14	0.20	56.9
49	71.28	9.77	9.64	9.49	1.08	1.07	1.08	13	13	14	0.19	57.1
50	72.28	9.57	9.90	9.69	1.10	1.09	1.10	13	14	14	0.22	57.3
51	73.28	9.77	9.92	9.84	1.10	1.09	1.08	13	14	14	0.19	57.4
52	74.28	9.83	9.99	10.0	1.08	1.09	1.08	14	14	14	0.17	57.6
53	75.28	9.92	9.76	9.92	1.10	1.07	1.08	14	14	14	0.18	57.8
54	76.28	9.93	9.83	9.79	1.08	1.09	1.07	13	14	14	0.19	57.9
55	77.28	9.89	9.92	10.0	1.07	1.09	1.09	13	13	14	0.24	58.1
56	78.28	9.98	9.92	10.2	1.07	1.10	1.07	13	14	14	0.20	58.2
57	79.28	10.1	9.61	10.0	1.08	1.07	1.09	13	13	14	0.13	58.4
58	80.28	9.95	10.1	10.1	1.09	1.09	1.06	13	14	14	0.17	58.5
59	81.28	10.1	10.3	10.2	1.08	1.09	1.10	14	14	14	0.20	58.6
60	82.28	10.2	10.3	10.1	1.08	1.08	1.11	14	14	14	0.21	58.8
61	83.28	10.1	10.2	10.1	1.07	1.08	1.09	14	14	14	0.17	58.9
62	84.28	10.3	10.2	10.3	1.09	1.06	1.10	14	14	13	0.19	59.0
63	85.28	10.0	10.2	10.1	1.08	1.09	1.09	13	13	13	0.18	59.1
64	86.28	10.3	10.3	10.4	1.09	1.09	1.07	14	14	13	0.21	59.2
65	87.28	10.4	10.4	10.2	1.09	1.10	1.10	14	14	13	0.18	59.4
66	88.28	10.4	10.5	10.4	1.07	1.09	1.10	13	14	13	0.19	59.5
67	89.28	10.6	10.3	10.6	1.09	1.08	1.09	14	14	14	0.17	59.6

Table D.1 – continued from previous page

test no	age [h]	unloading moduli [GPa]			unloading speed [kN/s]			number of data points			eccentricity [mm]	ξ [%]
68	90.28	10.6	10.7	10.4	1.09	1.08	1.10	14	14	14	0.19	59.7
69	91.28	10.3	10.4	10.5	1.07	1.10	1.09	13	14	14	0.24	59.8
70	92.28	10.4	10.6	10.5	1.08	1.09	1.10	13	13	14	0.16	59.9
71	93.28	10.5	10.6	10.8	1.08	1.09	1.10	13	14	14	0.22	60.0
72	94.28	10.4	10.5	10.4	1.09	1.09	1.10	14	13	14	0.19	60.1
73	95.28	10.5	10.8	10.9	1.09	1.09	1.09	14	13	13	0.21	60.2
74	96.28	10.6	10.4	10.5	1.09	1.10	1.09	14	14	13	0.21	60.3
75	97.28	10.6	10.6	10.8	1.09	1.08	1.08	13	14	14	0.23	60.4
76	98.28	10.5	10.5	10.5	1.09	1.07	1.09	13	13	13	0.22	60.4
77	99.28	10.6	10.6	10.5	1.11	1.09	1.09	14	13	14	0.19	60.5
78	100.3	10.6	10.8	10.5	1.11	1.08	1.09	14	14	13	0.19	60.6
79	101.3	10.4	10.7	10.6	1.10	1.09	1.07	13	13	14	0.26	60.7
80	102.3	10.6	10.6	10.6	1.07	1.10	1.08	13	14	14	0.22	60.8
81	103.3	10.6	10.7	10.8	1.07	1.07	1.06	14	13	14	0.15	60.8
82	104.3	10.5	10.8	10.7	1.07	1.08	1.06	14	14	14	0.25	60.9
83	105.3	10.7	10.7	10.5	1.08	1.07	1.08	14	13	13	0.22	61.0
84	106.3	10.8	10.8	10.6	1.09	1.08	1.09	14	14	14	0.19	61.1
85	107.3	10.7	10.6	10.9	1.09	1.08	1.07	14	13	14	0.21	61.1
86	108.3	10.7	10.8	10.6	1.08	1.09	1.08	14	14	14	0.17	61.2
87	109.3	10.9	10.7	10.9	1.10	1.08	1.08	13	14	14	0.17	61.3
88	110.3	10.8	10.8	10.7	1.07	1.10	1.09	13	14	13	0.24	61.3
89	111.3	10.8	10.9	10.8	1.08	1.10	1.09	13	14	13	0.19	61.4
90	112.3	10.9	10.7	10.7	1.09	1.08	1.09	13	13	13	0.19	61.5
91	113.3	10.9	10.7	10.8	1.10	1.09	1.07	14	13	14	0.17	61.5
92	114.3	11.0	10.9	10.8	1.08	1.09	1.07	13	14	14	0.15	61.6
93	115.3	10.9	11.0	10.8	1.10	1.08	1.09	14	14	14	0.17	61.6
94	116.3	11.1	11.0	11.0	1.09	1.09	1.10	14	14	14	0.13	61.7
95	117.3	10.9	11.0	10.7	1.08	1.09	1.09	14	14	13	0.23	61.8
96	118.7	11.0	10.9	10.9	1.10	1.11	1.07	14	14	14	1.3	61.8
97	119.7	10.8	11.0	11.0	1.09	1.08	1.10	14	14	14	1.3	61.9
98	120.7	10.8	10.8	10.8	1.10	1.08	1.07	14	14	14	1.3	61.9
99	121.7	11.0	11.0	11.0	1.08	1.07	1.09	14	14	14	1.3	62.0

Table D.1 – continued from previous page

test no	age [h]	unloading moduli [GPa]			unloading speed [kN/s]			number of data points			eccentricity [mm]	ξ [%]
100	122.7	10.8	10.7	11.1	1.09	1.08	1.07	14	14	14	1.3	62.0
101	123.7	10.9	10.9	11.1	1.08	1.07	1.10	14	14	14	1.3	62.1
102	124.7	10.9	10.9	10.8	1.07	1.09	1.08	15	14	14	1.3	62.1
103	125.7	10.9	10.9	10.9	1.07	1.07	1.10	14	15	14	1.3	62.2
104	126.7	11.0	11.0	10.9	1.08	1.07	1.08	14	14	14	1.3	62.2
105	127.7	10.8	10.9	10.8	1.08	1.09	1.07	14	14	15	1.3	62.3
106	128.7	11.0	10.9	11.1	1.07	1.06	1.08	15	15	14	1.3	62.3
107	129.7	10.9	10.9	11.1	1.05	1.06	1.08	15	15	14	1.3	62.4
108	130.7	11.2	10.9	11.2	1.08	1.09	1.08	15	14	14	1.3	62.4
109	131.7	10.9	10.9	11.0	1.05	1.05	1.07	15	15	14	1.3	62.5
110	132.7	10.9	11.1	11.0	1.08	1.06	1.07	14	15	15	1.3	62.5
111	133.7	10.8	11.1	11.1	1.07	1.08	1.09	14	14	14	1.3	62.5
112	134.7	11.2	11.1	10.9	1.09	1.08	1.08	14	15	14	1.3	62.6
113	135.7	11.0	11.0	11.0	1.06	1.08	1.08	15	14	14	1.3	62.6
114	136.7	11.0	11.1	11.2	1.08	1.09	1.08	15	14	14	1.3	62.7
115	137.7	11.0	11.3	10.8	1.09	1.07	1.09	14	15	14	1.3	62.7
116	138.7	10.9	11.0	11.3	1.07	1.07	1.08	15	15	15	1.3	62.8
117	139.7	11.3	11.1	11.3	1.07	1.08	1.08	14	14	14	1.3	62.8

Table D.2: Results from mechanical unloading tests on a cement paste sample with $w/s = w/c = 0.50$, produced on Nov 05, 2013, at 16h12; six orthogonal diameters were measured as 29.7, 29.9, 30.2, 30.1, 30.1 and 30.1 mm

test no	age [h]	unloading moduli [GPa]			unloading speed [kN/s]			number of data points			eccentricity [mm]	ξ [%]
1	25.74	5.24	5.36	5.31	1.08	1.08	1.06	13	14	14	0.95	38.0
2	26.74	5.42	5.43	5.40	1.08	1.07	1.09	14	14	13	0.95	38.9
3	27.74	5.60	5.63	5.59	1.06	1.08	1.07	14	13	13	0.96	39.7
4	28.74	5.82	5.83	5.81	1.07	1.08	1.08	14	14	14	0.94	40.5
5	29.74	5.96	5.96	6.03	1.07	1.07	1.05	14	14	14	0.95	41.2

Table D.2 – continued from previous page

test no	age [h]	unloading moduli [GPa]			unloading speed [kN/s]			number of data points			eccentricity [mm]	ξ [%]
6	30.74	6.17	6.22	6.13	1.07	1.05	1.08	14	14	14	0.94	42.0
7	31.74	6.25	6.21	6.30	1.08	1.08	1.08	14	13	14	0.95	42.6
8	32.74	6.48	6.45	6.46	1.07	1.06	1.04	14	14	14	0.94	43.3
9	33.74	6.63	6.74	6.64	1.08	1.07	1.05	14	14	14	0.93	43.9
10	34.74	6.75	6.73	6.81	1.07	1.08	1.06	14	14	14	0.94	44.5
11	35.74	6.95	6.95	6.93	1.05	1.06	1.08	14	14	13	0.91	45.1
12	36.74	7.00	7.12	7.04	1.08	1.09	1.07	14	14	14	0.95	45.7
13	37.74	7.17	7.14	7.13	1.07	1.07	1.06	14	13	14	0.91	46.2
14	38.74	7.21	7.37	7.28	1.07	1.09	1.07	13	14	14	0.95	46.7
15	39.74	7.50	7.42	7.34	1.09	1.09	1.08	13	14	14	0.91	47.2
16	40.74	7.53	7.48	7.49	1.08	1.10	1.09	14	13	13	0.93	47.6
17	41.74	7.57	7.55	7.63	1.10	1.08	1.07	13	13	13	0.92	48.2
18	42.74	7.72	7.69	7.69	1.06	1.07	1.07	14	14	14	0.91	48.7
19	43.74	7.71	7.76	7.73	1.08	1.08	1.08	14	13	13	0.91	49.1
20	44.74	7.68	7.84	7.89	1.09	1.08	1.08	14	14	14	0.92	49.5
21	45.74	7.71	7.80	7.78	1.09	1.08	1.07	13	14	14	0.95	50.0
22	46.74	8.00	8.06	7.99	1.07	1.07	1.07	14	14	13	0.93	50.4
23	47.74	8.00	7.99	8.12	1.08	1.04	1.11	14	14	14	0.92	50.8
24	48.74	8.02	8.16	8.25	1.09	1.07	1.08	14	14	14	0.93	51.1
25	49.74	8.22	8.15	8.21	1.09	1.10	1.07	14	14	14	0.91	51.5
26	50.74	8.41	8.39	8.24	1.07	1.07	1.07	14	14	14	0.94	51.9
27	51.74	8.36	8.42	8.27	1.07	1.07	1.07	14	14	14	0.92	52.2
28	52.74	8.44	8.55	8.54	1.08	1.07	1.06	14	14	14	0.95	52.5
29	53.74	8.45	8.60	8.58	1.08	1.08	1.21	13	14	11	0.92	52.9
30	54.74	8.72	8.54	8.48	1.07	1.08	1.06	14	14	13	0.93	53.2
31	55.74	8.66	8.76	8.60	1.07	1.08	1.08	14	14	14	0.91	53.5
32	56.74	8.63	8.75	8.64	1.09	1.07	1.09	14	14	14	0.92	53.8
33	57.74	8.81	8.85	8.83	1.07	1.07	1.09	14	14	14	0.90	54.1
34	58.74	8.81	8.90	8.88	1.07	1.08	1.07	14	14	14	0.91	54.3
35	59.74	8.84	9.07	9.01	1.08	1.07	1.07	14	14	14	0.94	54.6
36	60.74	9.08	8.97	8.97	1.09	1.10	1.07	13	13	14	0.94	54.9
37	61.74	8.89	8.97	9.00	1.09	1.09	1.08	14	14	14	0.94	55.1

Table D.2 – continued from previous page

test no	age [h]	unloading moduli [GPa]			unloading speed [kN/s]			number of data points			eccentricity [mm]	ξ [%]
38	62.74	9.08	9.15	9.07	1.07	1.07	1.07	14	14	14	0.92	55.3
39	63.74	9.08	9.17	9.22	1.09	1.08	1.08	14	14	14	0.89	55.6
40	64.74	9.13	9.22	9.22	1.08	1.10	1.08	14	14	13	0.93	55.8
41	65.74	9.12	9.12	9.23	1.09	1.09	1.07	13	14	14	0.94	56.0
42	66.74	9.42	9.39	9.29	1.08	1.07	1.09	14	14	14	0.90	56.2
43	67.74	9.35	9.40	9.17	1.09	1.09	1.09	14	14	14	0.91	56.4
44	68.74	9.37	9.35	9.42	1.10	1.09	1.10	14	13	14	0.92	56.6
45	69.74	9.31	9.24	9.26	1.08	1.09	1.10	14	14	14	0.94	56.8
46	70.74	9.42	9.45	9.42	1.07	1.07	1.09	14	14	14	0.92	57.0
47	71.74	9.55	9.41	9.53	1.08	1.09	1.10	15	14	15	0.94	57.2
48	72.74	9.59	9.55	9.52	1.08	1.04	1.08	14	14	14	0.94	57.4
49	73.74	9.43	9.63	9.61	1.08	1.08	1.09	14	14	14	0.93	57.5
50	74.74	9.67	9.59	9.57	1.07	1.09	1.07	14	15	14	0.93	57.7
51	75.74	9.82	9.73	9.80	1.08	1.09	1.10	14	14	14	0.94	57.8
52	76.74	9.67	9.69	9.75	1.07	1.10	1.08	14	14	14	0.94	58.0
53	77.74	9.49	10.0	9.56	1.07	1.09	1.08	14	14	13	0.95	58.1
54	78.74	9.71	9.83	9.95	1.07	1.08	1.09	14	14	14	0.92	58.3
55	79.74	9.78	9.85	9.89	1.09	1.10	1.09	14	14	14	0.93	58.4
56	80.74	10.0	9.83	10.0	1.09	1.07	1.08	14	14	14	0.95	58.6
57	81.74	9.92	9.87	9.95	1.08	1.09	1.09	13	14	14	0.91	58.7
58	82.74	9.87	10.0	9.96	1.10	1.08	1.10	14	14	13	0.96	58.8
59	83.74	9.98	10.0	10.1	1.08	1.08	1.11	14	14	13	0.93	58.9
60	84.74	10.1	10.0	9.97	1.07	1.08	1.08	14	14	14	0.90	59.1
61	85.74	10.0	10.2	9.94	1.09	1.09	1.08	14	14	14	0.91	59.2
62	86.74	9.98	10.2	10.1	1.08	1.09	1.07	14	13	14	0.93	59.3
63	87.74	10.4	10.1	10.2	1.08	1.07	1.07	13	14	14	0.92	59.4
64	88.74	9.98	9.99	10.2	1.08	1.06	1.07	14	14	14	0.95	59.5
65	89.74	10.3	10.0	10.1	1.08	1.08	1.06	14	14	14	0.93	59.6
66	90.74	10.3	10.1	10.3	1.08	1.10	1.07	15	13	14	0.93	59.7
67	91.74	10.3	10.3	10.3	1.08	1.10	1.10	14	14	13	0.89	59.8
68	92.74	10.1	10.2	10.3	1.10	1.07	1.10	14	14	13	0.97	59.9
69	93.74	10.2	10.2	10.4	1.09	1.08	1.07	14	14	14	0.95	60.0

Table D.2 – continued from previous page

test no	age [h]	unloading moduli [GPa]			unloading speed [kN/s]			number of data points			eccentricity [mm]	ξ [%]
70	94.74	10.5	10.6	10.5	1.08	1.09	1.06	14	13	14	0.96	60.1
71	95.74	10.3	10.2	10.1	1.08	1.10	1.08	13	13	14	0.98	60.2
72	96.74	10.5	10.3	10.6	1.08	1.08	1.08	14	14	14	0.93	60.3
73	97.74	10.3	10.6	10.3	1.08	1.08	1.08	14	14	14	0.96	60.4
74	98.74	10.3	10.4	10.4	1.07	1.10	1.08	14	13	14	0.96	60.5
75	99.74	10.7	10.4	10.5	1.08	1.08	1.06	13	13	14	0.93	60.6
76	100.7	10.4	10.4	10.2	1.08	1.08	1.08	14	14	14	0.96	60.6
77	101.7	10.2	10.6	10.4	1.08	1.08	1.15	13	14	13	0.94	60.7
78	102.7	10.5	10.4	10.3	1.09	1.09	1.07	13	14	13	0.97	60.8
79	103.7	10.3	10.3	10.4	1.07	1.08	1.07	14	14	14	0.93	60.9
80	104.7	10.5	10.4	10.5	1.07	1.07	1.07	14	14	14	0.97	60.9
81	105.7	10.5	10.7	10.4	1.08	1.07	1.09	13	14	14	0.98	61.0
82	106.7	10.7	10.6	10.5	1.09	1.10	1.07	13	14	14	0.98	61.1
83	107.7	10.4	10.6	10.5	1.10	1.08	1.10	14	14	13	0.96	61.2
84	108.7	10.7	10.6	10.6	1.08	1.08	1.06	13	13	14	0.94	61.2
85	109.7	10.4	10.7	10.5	1.09	1.07	1.08	13	14	14	0.99	61.3
86	110.7	10.4	11.0	10.8	1.09	1.09	1.09	14	14	14	0.96	61.4
87	111.7	10.8	11.0	10.7	1.09	1.09	1.08	14	14	13	0.95	61.4
88	112.7	10.6	10.6	10.5	1.08	1.09	1.07	14	14	14	0.97	61.5
89	113.7	10.7	10.7	10.7	1.09	1.08	1.10	13	14	14	0.98	61.5
90	114.7	10.7	10.9	10.8	1.08	1.10	1.07	13	13	14	0.97	61.6
91	115.7	10.6	11.0	10.8	1.07	1.08	1.07	14	14	14	0.97	61.7
92	116.7	10.9	10.6	10.7	1.10	1.09	1.08	13	14	14	0.95	61.7
93	117.7	10.8	10.8	10.7	1.07	1.08	1.08	14	14	13	0.95	61.8
94	118.7	10.7	10.7	10.7	1.09	1.05	1.09	14	13	14	0.96	61.8
95	119.7	11.0	10.8	10.8	1.08	1.07	1.08	14	14	13	0.94	61.9
96	120.7	11.1	10.7	10.7	1.08	1.07	1.08	14	14	14	0.95	61.9
97	121.7	10.8	10.7	10.7	1.07	1.08	1.08	14	14	14	0.93	62.0
98	122.7	10.6	10.6	10.9	1.09	1.08	1.10	13	14	14	0.97	62.0
99	123.7	11.1	10.6	10.8	1.08	1.10	1.10	14	13	14	0.94	62.1
100	124.7	10.9	11.0	11.0	1.06	1.10	1.09	14	13	14	0.95	62.1
101	125.7	10.7	11.0	11.1	1.09	1.07	1.04	13	14	13	0.97	62.2

Table D.2 – continued from previous page

test no	age [h]	unloading moduli [GPa]			unloading speed [kN/s]			number of data points			eccentricity [mm]	ξ [%]
102	126.7	10.8	11.1	10.9	1.09	1.08	1.08	13	14	13	0.98	62.2
103	127.7	10.9	10.9	10.8	1.09	1.10	1.08	14	13	13	0.98	62.3
104	128.7	11.0	11.0	11.1	1.10	1.08	1.09	13	14	14	0.96	62.3
105	129.7	10.9	10.7	11.1	1.10	1.07	1.10	14	14	14	0.95	62.4
106	130.7	10.8	11.0	11.0	1.08	1.08	1.08	13	14	14	0.98	62.4
107	131.7	10.9	11.0	10.7	1.09	1.08	1.09	14	13	14	0.98	62.5
108	132.7	11.1	11.1	11.0	1.07	1.07	1.07	14	14	14	0.95	62.5
109	133.7	11.2	11.2	11.2	1.08	1.08	1.07	14	14	14	0.97	62.6
110	134.7	11.0	11.2	11.0	1.10	1.07	1.08	13	14	13	0.94	62.6
111	135.7	10.9	11.1	10.9	1.08	1.07	1.08	14	14	14	1.00	62.6
112	136.7	11.1	11.1	11.3	1.09	1.07	1.08	14	14	14	0.96	62.7

Table D.3: Results from ultrasonics testing on a cement paste sample with $w/s = w/c = 0.50$, produced on Oct 28, 2013, at 11h21; six orthogonal diameters were measured as 29.7, 29.7, 29.9, 30.1, 29.7 and 30.1 mm

test no	age [h]	longitudinal wave speed [km/s]	shear wave speed [km/s]	dynamic Young's modulus [GPa]	ξ [%]
1	24.65	2.294	1.141	6.34	36.93
2	27.98	2.439	1.193	6.95	39.89
3	46.90	2.782	1.405	9.52	50.43
4	50.48	2.826	1.446	10.03	51.78
5	53.23	2.849	1.448	10.06	52.70
6	69.65	2.949	1.511	10.92	56.80
7	72.48	3.021	1.523	11.13	57.31
8	75.82	3.058	1.534	11.29	57.85

Table D.4: Results from ultrasonics testing on a cement paste sample with $w/s = w/c = 0.50$, produced on Nov 05, 2013, at 16h12; six orthogonal diameters were measured as 29.8, 29.4, 29.9, 29.8, 29.9 and 30.2 mm

test no	age [h]	longitudinal wave speed [km/s]	shear wave speed [km/s]	dynamic Young's modulus [GPa]	ξ [%]
1	24.97	2.379	1.147	6.57	37.24
2	41.30	2.706	1.364	9.15	47.99
3	44.30	2.739	1.389	9.46	49.35
4	47.55	2.813	1.416	9.84	50.67
5	64.97	2.998	1.468	10.64	55.85
6	68.47	3.008	1.490	10.91	56.58
7	70.80	3.012	1.498	11.02	57.01
8	89.30	3.088	1.531	11.53	59.59
9	91.80	3.088	1.541	11.60	59.84

Table D.5: Results from mechanical unloading tests on a cement paste sample with $w/s = w/c = 0.42$, produced on Oct 21, 2013, at 09h41; six orthogonal diameters were measured as 29.9, 29.9, 30.2, 29.9, 30.0 and 29.9 mm

test no	age [h]	unloading moduli [GPa]			unloading speed [kN/s]			number of data points			eccentricity [mm]	ξ [%]
1	25.58	7.90	7.85	7.77	1.05	1.05	1.01	14	14	13	0.032	36.8
2	26.58	8.05	8.10	8.11	1.07	1.07	1.05	14	14	15	0.063	37.7
3	27.58	8.20	8.20	8.33	1.07	1.07	1.06	14	14	14	0.043	38.6
4	28.58	8.39	8.39	8.40	1.07	1.06	1.06	14	14	15	0.09	39.4
5	29.58	8.63	8.81	8.49	1.06	1.06	1.06	14	14	13	0.059	40.1
6	30.58	8.74	8.82	8.75	1.08	1.07	1.07	14	14	14	0.064	40.8
7	31.58	8.99	8.97	8.93	1.06	1.06	1.07	15	14	14	0.018	41.5
8	32.58	9.23	9.10	9.20	1.06	1.08	1.07	14	14	14	0.023	42.2
9	33.58	9.20	9.21	9.20	1.05	1.07	1.07	14	14	14	0.071	42.8

Table D.5 – continued from previous page

test no	age [h]	unloading moduli [GPa]			unloading speed [kN/s]			number of data points			eccentricity [mm]	ξ [%]
10	34.58	9.31	9.46	9.36	1.07	1.07	1.07	14	14	14	0.068	43.4
11	35.58	9.64	9.24	9.59	1.08	1.07	1.06	14	14	14	0.024	44.0
12	36.58	9.59	9.60	9.61	1.08	1.08	1.07	14	14	14	0.041	44.5
13	37.58	9.82	9.64	9.81	1.08	1.06	1.06	14	15	14	0.04	45.1
14	38.58	10.0	9.98	9.93	1.06	1.06	1.07	14	14	13	0.075	45.6
15	39.58	10.2	10.1	9.89	1.06	1.06	1.08	14	14	14	0.063	46.1
16	40.58	9.96	10.2	10.4	1.07	1.06	1.06	13	14	14	0.061	46.6
17	41.58	10.2	10.2	10.3	1.08	1.06	1.07	13	14	14	0.041	47.1
18	42.58	10.6	10.6	10.3	1.08	1.06	1.06	14	14	14	0.016	47.6
19	43.58	10.7	10.3	10.5	1.07	1.07	1.06	14	14	15	0.032	48.0
20	44.58	10.7	10.6	10.5	1.06	1.06	1.06	14	14	14	0.037	48.5
21	45.58	10.7	10.8	10.8	1.06	1.06	1.07	13	14	14	0.038	48.9
22	46.58	10.6	11.0	10.9	1.08	1.07	1.08	14	14	14	0.074	49.3
23	47.58	10.8	11.0	10.7	1.07	1.07	1.05	14	14	13	0.046	49.7
24	48.58	11.0	11.1	10.9	1.07	1.07	1.06	13	14	13	0.038	50.1
25	49.58	10.9	10.9	11.0	1.09	1.06	1.03	14	13	13	0.075	50.5
26	50.58	11.3	11.1	11.1	1.09	1.08	1.07	14	14	13	0.051	50.9
27	51.58	11.2	11.2	11.1	1.08	1.07	1.07	14	14	13	0.072	51.2
28	52.58	11.2	11.3	11.2	1.07	1.07	1.07	14	14	14	0.072	51.5
29	53.58	11.0	11.5	11.5	1.07	1.07	1.08	14	14	14	0.13	51.9
30	54.58	11.5	11.4	11.2	1.08	1.07	1.08	14	13	14	0.018	52.2
31	55.58	11.4	11.3	11.6	1.06	1.08	1.07	14	14	14	0.087	52.5
32	56.58	11.6	11.6	11.4	1.07	1.08	1.06	13	14	14	0.054	52.8
33	57.58	11.6	11.5	11.6	1.07	1.06	1.07	14	14	14	0.018	53.1
34	58.58	11.7	11.7	11.7	1.07	1.07	1.06	14	14	14	0.083	53.4
35	59.58	11.8	11.7	11.7	1.08	1.08	1.07	14	14	14	0.099	53.6
36	60.58	11.9	11.7	11.8	1.07	1.07	1.07	13	14	14	0.085	53.9
37	61.58	11.7	12.0	11.6	1.08	1.06	1.07	14	14	14	0.038	54.1
38	62.58	11.9	11.8	12.0	1.08	1.06	1.08	14	15	14	0.036	54.4
39	63.58	12.0	11.7	12.0	1.06	1.07	1.06	14	14	14	0.07	54.6
40	64.58	11.9	12.0	11.9	1.06	1.08	1.06	14	14	14	0.093	54.8
41	65.58	12.3	12.0	12.4	1.07	1.06	1.07	13	15	13	0.11	55.1

Table D.5 – continued from previous page

test no	age [h]	unloading moduli [GPa]			unloading speed [kN/s]			number of data points			eccentricity [mm]	ξ [%]
42	66.58	12.3	12.1	12.1	1.08	1.07	1.06	14	14	15	0.038	55.3
43	67.58	12.1	12.1	12.4	1.07	1.08	1.07	14	14	13	0.073	55.5
44	68.58	12.4	12.5	12.2	1.06	1.07	1.07	14	14	14	0.039	55.7
45	69.58	12.5	12.2	12.4	1.06	1.08	1.06	14	14	14	0.082	55.9
46	70.58	12.3	12.5	12.4	1.07	1.08	1.06	14	14	14	0.073	56.1
47	71.58	12.4	12.4	12.4	1.07	1.08	1.05	14	14	14	0.078	56.2
48	72.58	12.6	12.4	12.6	1.07	1.08	1.08	14	14	14	0.036	56.4
49	73.58	12.5	12.5	12.5	1.07	1.06	0.98	14	14	13	0.045	56.6
50	74.58	12.6	12.7	12.5	1.07	1.07	1.07	14	14	14	0.049	56.7
51	75.58	13.0	12.7	12.8	1.09	1.08	1.07	14	14	13	0.036	56.9
52	76.58	13.0	12.6	12.6	1.08	1.05	1.07	14	14	14	0.027	57.1
53	77.58	12.7	12.7	12.7	1.08	1.07	1.07	14	14	14	0.015	57.2
54	78.58	12.8	12.7	12.7	1.07	1.07	1.08	14	14	14	0.081	57.3
55	79.58	12.6	12.7	12.9	1.07	1.07	1.07	14	14	14	0.077	57.5
56	80.58	12.8	12.7	12.8	1.08	1.06	1.07	14	14	15	0.0034	57.6
57	81.58	12.6	13.0	12.7	1.08	1.07	1.07	14	14	14	0.058	57.8
58	82.58	12.6	12.5	12.7	1.07	1.07	1.07	14	15	15	0.081	57.9
59	83.58	13.0	12.8	13.1	1.08	1.08	1.07	14	14	14	0.069	58.0
60	84.58	13.1	12.9	12.9	1.07	1.08	1.07	14	14	14	0.084	58.1
61	85.58	13.0	12.5	12.8	1.07	1.09	1.06	14	14	15	0.077	58.3
62	86.58	13.0	13.0	12.9	1.07	1.06	1.06	13	14	15	0.076	58.4
63	87.58	13.0	12.9	12.6	1.07	1.07	1.07	14	14	14	0.084	58.5
64	88.58	13.3	13.2	12.9	1.07	1.08	1.07	14	14	14	0.11	58.6
65	89.58	13.2	13.0	13.1	1.07	1.07	1.06	14	13	14	0.078	58.7
66	90.58	12.9	13.1	13.2	1.08	1.08	1.06	14	14	14	0.066	58.8
67	91.58	13.0	13.0	13.5	1.07	1.07	1.07	14	14	14	0.089	58.9
68	92.58	13.1	13.2	13.2	1.07	1.06	1.07	14	14	14	0.02	59.0
69	93.58	13.3	13.2	13.2	1.07	1.07	1.07	14	14	14	0.10	59.1
70	94.58	13.0	13.1	13.1	1.07	1.08	1.07	14	14	13	0.13	59.2
71	95.58	13.0	12.9	12.9	1.06	1.07	1.07	14	13	14	0.14	59.3
72	96.58	13.2	13.4	13.1	1.07	1.07	1.07	14	13	14	0.11	59.3
73	97.58	13.1	13.2	13.3	1.08	1.07	1.15	14	14	12	0.10	59.4

Table D.6: Results from mechanical unloading tests on a
cement paste sample with $w/s = w/c = 0.42$, produced
on Oct 24, 2013, at 11h43; six orthogonal diameters were
measured as 30.1, 29.9, 30.1, 29.8, 29.8 and 29.8 mm

test no	age [h]	unloading moduli [GPa]			unloading speed [kN/s]			number of data points			eccentricity [mm]	ξ [%]
1	25.1	7.88	7.84	7.90	1.06	1.06	1.06	14	15	14	0.10	36.3
2	26.1	8.08	8.20	8.13	1.07	1.06	1.06	14	15	15	0.13	37.3
3	27.1	8.22	8.28	8.54	0.95	1.08	1.06	11	14	15	0.11	38.2
4	28.1	8.48	8.60	8.41	1.06	1.07	1.08	15	15	14	0.10	39.0
5	29.1	8.83	8.88	8.74	1.07	1.07	1.07	14	14	14	0.084	39.7
6	30.1	9.07	9.04	8.99	1.08	1.08	1.07	15	14	14	0.089	40.5
7	31.1	9.18	9.19	9.08	1.09	1.06	1.05	15	14	14	0.12	41.2
8	32.1	9.26	9.27	9.14	1.07	1.07	1.08	14	14	14	0.094	41.9
9	33.1	9.51	9.38	9.30	1.07	1.10	1.07	15	14	15	0.12	42.5
10	34.1	9.59	9.47	9.48	1.08	1.04	1.07	15	14	14	0.067	43.1
11	35.1	9.68	9.62	9.59	1.08	1.09	1.07	15	14	14	0.08	43.7
12	36.1	9.81	9.77	9.62	1.09	1.07	1.07	14	14	14	0.11	44.3
13	37.1	9.74	9.86	9.72	1.06	1.06	1.07	14	15	15	0.073	44.8
14	38.1	9.89	9.92	9.84	1.07	1.07	1.07	14	14	15	0.08	45.4
15	39.1	10.1	10.1	9.77	1.08	1.05	1.06	14	14	14	0.076	45.9
16	40.1	10.3	10.4	10.3	1.08	1.06	1.31	15	15	10	0.061	46.4
17	41.1	10.4	10.4	10.3	1.09	1.08	1.07	15	15	14	0.062	46.9
18	42.1	10.5	10.4	10.4	1.08	1.08	1.08	15	15	15	0.083	47.4
19	43.1	10.7	10.5	10.5	1.08	1.06	1.08	15	14	15	0.083	47.8
20	44.1	10.7	10.6	10.6	1.07	1.06	1.07	14	14	14	0.074	48.3
21	45.1	10.8	10.7	10.6	1.06	1.07	1.07	14	15	15	0.044	48.7
22	46.1	10.8	11.0	10.7	1.08	1.09	1.06	14	15	14	0.055	49.1
23	47.1	11.0	11.0	11.1	1.06	1.05	1.08	14	14	14	0.082	49.5
24	48.1	11.4	11.0	11.2	1.08	1.08	1.06	15	14	14	0.093	49.9
25	49.1	11.1	11.2	11.5	1.07	1.08	1.09	14	14	15	0.07	50.3
26	50.1	11.4	11.3	11.6	1.09	1.06	1.09	14	14	15	0.081	50.7
27	51.1	11.6	11.6	11.2	1.07	1.06	1.07	14	14	14	0.11	51.0

Table D.6 – continued from previous page

test no	age [h]	unloading moduli [GPa]			unloading speed [kN/s]			number of data points			eccentricity [mm]	ξ [%]
28	52.1	11.3	11.5	11.6	1.07	1.08	1.07	14	15	15	0.087	51.4
29	53.1	11.5	11.7	11.5	1.09	1.09	1.07	14	15	14	0.083	51.7
30	54.1	11.5	12.0	11.6	1.08	1.08	1.08	14	14	14	0.12	52.0
31	55.1	11.8	12.0	11.9	1.08	1.05	1.07	14	14	15	0.056	52.4
32	56.1	11.7	12.0	11.8	1.06	1.07	1.07	14	15	15	0.11	52.7
33	57.1	11.9	12.1	11.9	1.08	1.07	1.07	14	14	14	0.11	52.9
34	58.1	11.9	12.1	11.9	1.09	1.06	1.08	14	14	14	0.094	53.2
35	59.1	12.0	12.0	12.1	1.08	1.09	1.07	14	15	14	0.11	53.5
36	60.1	12.1	12.2	12.0	1.07	1.08	1.06	14	15	14	0.12	53.8
37	61.1	12.2	12.1	12.0	1.08	1.08	1.06	15	15	14	0.071	54.0
38	62.1	12.2	12.3	12.1	1.09	1.08	1.07	14	15	14	0.13	54.3
39	63.1	12.3	11.9	12.5	1.08	1.07	1.09	15	14	14	0.073	54.5
40	64.1	12.5	12.4	12.3	1.13	1.07	1.07	11	14	14	0.10	54.7
41	65.1	12.2	12.3	12.4	1.08	1.07	1.08	15	14	14	0.13	55.0
42	66.1	12.3	12.3	12.5	1.06	1.08	1.08	15	14	14	0.09	55.2
43	67.1	12.6	12.5	12.5	1.08	1.07	1.08	15	14	15	0.081	55.4
44	68.1	12.3	12.4	12.4	1.06	1.06	1.08	14	14	14	0.11	55.6
45	69.1	12.9	12.8	12.7	1.08	1.10	1.06	14	14	14	0.13	55.8
46	70.1	12.7	12.9	12.8	1.07	1.07	1.07	14	15	14	0.11	56.0
47	71.1	12.6	12.8	12.5	1.07	1.07	1.05	14	15	14	0.08	56.1
48	72.1	12.7	12.9	12.8	1.09	1.09	1.06	14	14	15	0.08	56.3
49	73.1	12.8	12.8	13.0	1.08	1.07	1.06	14	14	14	0.067	56.5
50	74.1	12.8	12.9	12.8	1.08	1.09	1.07	15	14	14	0.11	56.7
51	75.1	12.8	12.9	13.0	1.06	1.06	1.08	14	14	15	0.098	56.8
52	76.1	12.9	13.2	12.8	1.10	1.09	1.07	14	15	15	0.08	57.0
53	77.1	13.0	12.9	12.9	1.07	1.08	1.08	14	14	14	0.08	57.1
54	78.1	12.9	12.8	13.1	1.09	1.07	1.07	14	14	14	0.08	57.3
55	79.1	13.2	13.0	13.0	1.07	1.08	1.08	14	15	15	0.14	57.4
56	80.1	12.8	13.2	13.3	1.07	1.08	1.08	14	14	14	0.081	57.6
57	81.1	13.4	12.9	13.2	1.08	1.07	1.05	15	14	14	0.096	57.7
58	82.1	13.3	12.9	13.1	1.07	1.09	1.05	14	14	14	0.072	57.8
59	83.1	12.9	13.2	13.1	1.08	1.07	1.08	14	14	14	0.067	58.0

Table D.6 – continued from previous page

test no	age [h]	unloading moduli [GPa]			unloading speed [kN/s]			number of data points			eccentricity [mm]	ξ [%]
60	84.1	13.2	13.1	13.0	1.09	1.07	1.06	15	14	14	0.071	58.1
61	85.1	13.2	13.3	13.2	1.07	1.06	1.10	14	14	14	0.083	58.2
62	86.1	13.3	13.1	13.5	1.08	1.08	1.08	15	14	15	0.047	58.3
63	87.1	13.6	13.1	13.1	1.08	1.07	1.07	14	14	14	0.13	58.4
64	88.1	13.4	13.5	13.4	1.07	1.08	1.07	15	14	14	0.071	58.5
65	89.1	13.2	13.6	13.3	1.07	1.08	1.06	14	15	15	0.07	58.6
66	90.1	13.2	13.3	13.5	1.05	1.09	1.07	15	14	15	0.12	58.7
67	91.1	13.2	13.3	13.3	1.08	1.07	1.08	14	14	15	0.078	58.8
68	92.1	13.5	13.4	13.4	1.08	1.07	1.08	14	15	14	0.12	58.9
69	93.1	13.3	13.2	13.5	1.06	1.08	1.07	14	14	14	0.13	59.0
70	94.1	13.4	13.4	13.5	1.08	1.06	1.08	15	14	15	0.11	59.1
71	95.1	13.4	13.5	13.3	1.08	1.08	1.07	14	15	14	0.10	59.2
72	96.1	13.3	13.4	13.3	1.08	1.07	1.06	15	15	14	0.13	59.3
73	97.1	13.7	13.4	13.5	1.08	1.07	1.07	15	14	14	0.08	59.4
74	98.1	13.3	13.5	13.5	1.06	1.07	1.07	14	14	15	0.044	59.5
75	99.1	13.5	13.2	13.3	1.07	1.10	1.07	14	14	15	0.02	59.5
76	100.1	13.5	13.2	13.4	1.08	1.08	1.07	14	14	14	0.12	59.6
77	101.1	13.6	13.2	13.1	1.07	1.08	1.08	15	14	15	0.096	59.7
78	102.1	13.5	13.6	13.5	1.08	1.08	1.07	15	15	15	0.093	59.8
79	103.1	13.2	13.8	13.0	1.09	1.08	1.06	14	14	15	0.084	59.9
80	104.1	13.4	13.6	13.3	1.07	1.07	1.07	14	15	14	0.12	59.9
81	105.1	13.8	13.6	13.5	1.08	1.08	1.07	14	15	14	0.095	60.0
82	106.1	13.5	13.6	13.7	1.07	1.06	1.07	15	14	15	0.08	60.1
83	107.1	13.1	13.4	13.6	1.06	1.07	1.07	14	15	15	0.093	60.1
84	108.1	13.6	13.6	13.5	1.07	1.06	1.05	14	14	14	0.034	60.2
85	109.1	13.2	13.3	13.5	1.06	1.08	1.05	14	14	14	0.12	60.3
86	110.1	13.0	13.3	13.6	1.09	1.07	1.08	14	15	15	0.084	60.3
87	111.1	13.6	13.7	13.6	1.07	1.10	1.06	15	14	15	0.093	60.4
88	112.1	13.3	13.7	13.4	1.07	1.08	1.08	14	14	14	0.093	60.4
89	113.1	13.8	13.4	13.4	1.09	1.07	1.07	10	14	14	0.13	60.5
90	114.1	13.4	13.4	13.4	1.08	1.06	1.06	14	14	14	0.10	60.6
91	115.1	13.4	13.6	13.6	1.08	1.09	1.08	14	14	15	0.12	60.6

Table D.6 – continued from previous page

test no	age [h]	unloading moduli [GPa]			unloading speed [kN/s]			number of data points			eccentricity [mm]	ξ [%]
92	116.1	13.7	13.5	13.7	1.10	1.09	1.09	15	14	15	0.093	60.7
93	117.1	13.6	13.6	13.7	1.07	1.08	1.07	15	14	14	0.08	60.7
94	118.1	13.7	13.4	13.2	1.09	1.07	1.08	15	15	14	0.081	60.8

Table D.7: Results from ultrasonics testing on a cement paste sample with $w/s = w/c = 0.42$, produced on Oct 21, 2013, at 09h41; six orthogonal diameters were measured as 30.1, 30.0, 30.3, 30.2, 30.2 and 30.0 mm

test no	age [h]	longitudinal wave speed [km/s]	shear wave speed [km/s]	dynamic Young's modulus [GPa]	ξ [%]
1	26.15	2.751	1.390	9.85	37.33
2	27.65	2.813	1.404	10.06	38.61
3	32.07	2.828	1.455	10.68	41.83
4	48.07	3.071	1.546	12.13	49.92
5	52.40	3.099	1.581	12.60	51.49
6	55.32	3.153	1.591	12.80	52.42
7	71.40	3.164	1.675	13.93	56.20
8	74.48	3.175	1.695	14.20	56.73
9	77.65	3.211	1.699	14.32	57.21
10	96.98	3.365	1.745	15.30	59.38

Table D.8: Results from ultrasonics testing on a cement paste sample with $w/s = w/c = 0.42$, produced on Oct 24, 2013, at 11h43; six orthogonal diameters were measured as 29.9, 30.0, 29.9, 29.9, 30.0 and 29.9 mm

test no	age [h]	longitudinal wave speed [km/s]	shear wave speed [km/s]	dynamic Young's modulus [GPa]	ξ [%]
1	26.12	2.710	1.374	9.59	37.30
2	27.78	2.871	1.403	10.13	38.72
3	94.53	3.239	1.695	14.42	59.16
4	97.87	3.366	1.713	14.87	59.45

Table D.9: Results from mechanical unloading tests on a cement paste sample with $w/s = 0.42$ and $w/c = 0.50$, produced on Nov 14, 2013, at 10h29; six orthogonal diameters were measured as 30.3, 29.6, 30.0, 29.6, 29.6 and 29.7 mm

test no	age [h]	unloading moduli [GPa]			unloading speed [kN/s]			number of data points			eccentricity [mm]	ξ [%]
1	25.87	7.26	7.25	7.17	0.986	0.998	0.977	16	15	16	0.38	38.8
2	26.87	7.62	7.34	7.60	1.000	0.991	0.974	15	16	16	0.41	39.7
3	27.87	7.65	7.69	7.68	0.974	0.997	1.000	16	16	16	0.41	40.6
4	28.87	7.91	7.99	7.78	0.992	1.000	0.992	16	15	16	0.36	41.4
5	29.87	8.03	8.09	7.98	0.990	0.977	0.997	16	16	16	0.37	42.1
6	30.87	8.08	8.14	8.13	0.994	0.986	0.997	16	16	16	0.40	42.9
7	31.87	8.44	8.33	8.54	1.020	0.998	1.000	15	16	15	0.40	43.5
8	32.87	8.51	8.43	8.57	1.000	0.983	0.973	16	16	16	0.36	44.2
9	33.87	8.59	8.63	8.72	0.998	0.986	1.000	16	16	15	0.42	44.8
10	34.87	8.95	8.66	8.82	1.000	0.980	0.994	15	16	16	0.42	45.4
11	35.87	9.02	8.92	9.15	1.020	0.980	0.990	15	16	15	0.40	46.0
12	36.87	9.20	9.22	8.96	1.010	1.010	0.996	15	15	16	0.37	46.5
13	37.87	9.15	9.46	9.20	0.979	1.010	1.010	16	15	15	0.38	47.1
14	38.87	9.35	9.37	9.17	0.987	0.981	0.985	16	15	16	0.38	47.6

Table D.9 – continued from previous page

test no	age [h]	unloading moduli [GPa]			unloading speed [kN/s]			number of data points			eccentricity [mm]	ξ [%]
15	39.87	9.25	9.31	9.34	1.020	0.997	0.991	15	15	16	0.36	48.1
16	40.87	9.41	9.57	9.44	0.994	0.987	0.984	16	16	16	0.39	48.6
17	41.87	9.53	9.57	9.73	1.010	0.978	0.991	16	16	15	0.39	49.0
18	42.87	9.62	9.52	9.64	1.010	0.970	0.976	16	16	16	0.39	49.5
19	43.87	10.0	9.74	9.73	1.020	0.982	0.980	15	16	16	0.41	49.9
20	44.87	9.99	9.72	9.83	1.000	0.989	1.000	15	15	15	0.42	50.3
21	45.87	10.0	9.94	9.88	1.020	0.982	0.999	15	16	16	0.34	50.7
22	46.87	10.2	10.0	10.0	0.998	0.993	0.981	15	15	16	0.38	51.1
23	47.87	10.4	10.1	10.4	1.020	0.965	1.010	15	16	15	0.40	51.5
24	48.87	10.3	10.2	10.3	0.978	0.982	0.993	15	16	15	0.42	51.8
25	49.87	10.4	10.6	10.4	1.020	1.010	0.987	15	15	16	0.40	52.2
26	50.87	10.2	10.3	10.4	0.998	0.990	0.983	16	16	16	0.36	52.5
27	51.87	10.4	10.6	10.6	0.994	1.000	1.000	15	15	15	0.45	52.9
28	52.87	10.6	10.8	10.5	1.010	1.010	0.996	15	15	15	0.41	53.2
29	53.87	10.7	10.9	10.9	0.995	1.010	0.978	15	15	15	0.46	53.5
30	54.87	10.6	10.4	10.6	0.982	0.979	0.988	16	16	16	0.41	53.8
31	55.87	10.5	10.6	10.6	0.982	0.960	0.980	16	16	16	0.42	54.1
32	56.87	10.9	10.9	10.7	0.987	1.010	0.965	15	15	16	0.45	54.4
33	57.87	11.0	10.8	10.8	0.998	0.988	1.010	15	15	15	0.40	54.7
34	58.87	10.9	10.8	10.8	0.990	0.975	1.010	16	16	15	0.39	54.9
35	59.87	10.8	11.2	10.8	0.984	0.977	0.991	16	16	16	0.41	55.2
36	60.87	11.1	11.3	11.2	0.986	0.997	0.984	15	15	16	0.47	55.4
37	61.87	11.0	11.1	11.1	0.989	0.982	0.964	16	16	16	0.42	55.7
38	62.87	11.3	11.2	11.1	1.010	0.983	0.985	15	16	16	0.43	55.9
39	63.87	11.1	11.2	11.3	0.990	0.999	1.010	16	15	15	0.46	56.1
40	64.87	11.4	11.1	11.1	0.968	0.988	0.993	16	16	16	0.39	56.4
41	65.87	11.3	11.8	11.2	0.984	0.987	0.984	16	15	16	0.46	56.6
42	66.87	11.5	11.3	11.5	1.000	0.978	0.978	15	16	16	0.43	56.8
43	67.87	11.6	11.6	11.6	0.987	0.979	0.990	16	16	15	0.46	57.0
44	68.87	11.6	11.4	11.5	1.010	0.976	0.982	15	16	16	0.49	57.2
45	69.87	11.7	11.5	11.5	1.010	0.984	0.976	15	16	16	0.50	57.4
46	70.87	11.4	11.5	11.5	0.976	0.974	0.977	16	16	16	0.45	57.6

Table D.9 – continued from previous page

test no	age [h]	unloading moduli [GPa]			unloading speed [kN/s]			number of data points			eccentricity [mm]	ξ [%]
47	71.87	11.7	11.8	12.0	0.983	0.988	1.000	16	15	15	0.44	57.7
48	72.87	11.7	11.7	11.9	0.991	0.980	1.000	16	16	15	0.45	57.9
49	73.87	11.9	11.8	11.9	0.987	1.000	0.984	15	15	15	0.43	58.1
50	74.87	11.8	12.0	11.7	0.984	0.977	0.984	15	15	15	0.41	58.2
51	75.87	11.8	11.7	11.9	0.984	0.983	0.998	16	16	15	0.47	58.4
52	76.87	12.0	11.7	11.8	0.997	0.992	0.992	15	16	16	0.45	58.6
53	77.87	12.0	12.0	12.1	0.981	0.986	0.994	16	15	15	0.46	58.7
54	78.87	12.3	11.8	12.2	1.000	0.986	1.010	15	16	15	0.51	58.8
55	79.87	12.0	12.2	12.1	0.997	1.010	0.969	16	15	16	0.44	59.0
56	80.87	12.2	11.8	11.9	0.994	0.985	0.980	15	15	16	0.50	59.1
57	81.87	12.0	12.0	12.0	0.982	1.000	0.969	15	15	16	0.44	59.2
58	82.87	11.9	12.4	12.1	0.988	1.010	0.990	16	15	16	0.50	59.4
59	83.87	12.1	12.3	12.2	0.982	0.991	0.980	16	15	16	0.47	59.5
60	84.87	12.3	12.4	12.0	1.010	1.000	0.991	15	15	16	0.50	59.6
61	85.87	12.3	12.3	12.2	1.000	0.986	0.988	15	16	15	0.45	59.7
62	86.87	12.2	12.2	11.9	0.991	0.999	0.975	14	15	16	0.50	59.9
63	87.87	12.3	12.5	12.1	0.999	0.995	0.990	15	15	16	0.53	60.0
64	88.87	12.3	12.2	12.4	1.000	0.988	0.986	15	16	16	0.54	60.1
65	89.87	12.2	12.3	12.3	0.987	0.985	0.967	15	16	16	0.54	60.2
66	90.87	12.0	12.2	12.1	0.969	0.980	0.970	15	15	16	0.52	60.3
67	91.87	12.2	12.6	12.2	0.974	1.010	1.000	15	15	15	0.53	60.4
68	92.87	12.5	12.1	12.1	0.988	0.982	0.958	14	16	15	0.45	60.5
69	93.87	12.6	12.3	12.3	1.020	0.991	1.000	15	16	15	0.50	60.6
70	94.87	12.6	12.7	12.7	0.991	1.010	0.998	15	15	15	0.54	60.7

Table D.10: Results from mechanical unloading tests on
a cement paste sample with $w/s = 0.42$ and $w/c = 0.50$,
produced on Nov 27, 2013, at 15h52; six orthogonal di-
ameters were measured as 29.4, 29.4, 29.8, 29.9, 29.7 and
29.5 mm

test no	age [h]	unloading moduli [GPa]			unloading speed [kN/s]			number of data points			eccentricity [mm]	ξ [%]
1	24.84	6.90	7.18	6.86	1.00	1.03	1.01	15	15	15	0.095	37.8
2	25.84	7.20	7.14	7.12	1.01	0.98	1.00	14	15	16	0.13	38.8
3	26.84	7.46	7.58	7.45	1.00	1.00	0.99	15	15	15	0.10	39.7
4	27.84	7.59	7.75	7.72	1.00	1.03	1.02	14	14	15	0.11	40.5
5	28.84	7.97	7.85	7.72	1.01	0.99	1.02	14	16	15	0.13	41.4
6	29.84	8.00	8.02	8.01	1.02	1.00	1.02	15	15	15	0.12	42.1
7	30.84	8.11	8.33	8.15	1.01	1.04	1.02	15	14	14	0.10	42.8
8	31.84	8.33	8.46	8.25	1.04	1.01	1.01	14	15	14	0.072	43.5
9	32.84	8.50	8.34	8.52	1.03	1.01	1.01	14	14	15	0.10	44.2
10	33.84	8.61	8.59	8.79	0.99	1.02	1.01	15	15	15	0.11	44.8
11	34.84	8.65	8.73	8.82	1.02	1.02	1.02	15	14	15	0.12	45.4
12	35.84	8.81	8.89	8.73	1.01	1.02	1.02	14	15	15	0.088	46.0
13	36.84	8.98	8.91	9.06	1.02	1.02	1.02	15	15	14	0.11	46.5
14	37.84	9.15	9.25	9.28	1.01	1.01	1.00	14	14	14	0.12	47.1
15	38.84	9.29	9.25	9.20	1.02	1.02	1.02	14	15	14	0.10	47.6
16	39.84	9.41	9.26	9.34	1.02	1.01	1.01	14	14	14	0.10	48.1
17	40.84	9.32	9.33	9.56	1.01	1.00	1.00	14	14	14	0.11	48.6
18	41.84	9.53	9.44	9.57	0.99	1.00	1.01	14	14	14	0.11	49
19	42.84	9.62	9.64	9.62	1.01	1.01	1.02	14	14	15	0.085	49.5
20	43.84	9.62	9.87	9.48	1.02	1.02	1.00	14	15	15	0.08	49.9
21	44.84	9.97	9.93	9.74	1.01	1.00	1.01	14	14	14	0.12	50.3
22	45.84	10.0	9.86	10.0	1.01	1.02	1.02	14	14	15	0.12	50.7
23	46.84	10.1	10.1	9.92	1.02	1.02	1.02	14	15	15	0.07	51.1
24	47.84	10.2	10.1	10.1	1.01	1.03	1.01	14	14	14	0.11	51.5
25	48.84	9.99	10.3	10.3	1.02	1.02	1.03	15	14	14	0.11	51.8
26	49.84	10.4	10.3	10.3	1.02	1.02	1.00	14	15	14	0.13	52.2
27	50.84	10.4	10.5	10.1	1.01	1.02	1.02	14	15	15	0.091	52.5
28	51.84	10.4	10.3	10.6	1.03	1.02	1.03	14	14	14	0.054	52.9

Table D.10 – continued from previous page

test no	age [h]	unloading moduli [GPa]			unloading speed [kN/s]			number of data points			eccentricity [mm]	ξ [%]
29	52.84	10.6	10.6	10.6	1.02	1.01	1.03	14	14	14	0.048	53.2
30	53.84	10.8	10.7	10.4	1.02	1.03	1.02	15	14	15	0.13	53.5
31	54.84	10.6	10.6	10.6	1.02	1.01	1.02	14	14	15	0.08	53.8
32	55.84	10.7	10.5	10.6	1.01	1.03	1.01	14	14	14	0.077	54.1
33	56.84	10.7	10.6	10.8	1.00	1.01	1.03	14	15	15	0.095	54.4
34	57.84	10.8	10.8	10.7	1.03	1.01	1.02	14	14	15	0.09	54.7
35	58.84	11.1	10.9	11.1	1.02	1.03	1.02	14	14	14	0.14	54.9
36	59.84	11.0	11.0	10.9	1.02	1.02	1.02	14	15	14	0.078	55.2
37	60.84	11.0	11.0	10.8	1.02	1.03	1.02	14	14	15	0.077	55.4
38	61.84	11.0	11.1	11.0	1.03	1.03	1.02	14	14	14	0.077	55.7
39	62.84	11.2	11.2	11.2	1.02	1.03	1.01	15	14	14	0.11	55.9
40	63.84	11.3	11.1	11.3	1.01	1.03	1.00	14	15	14	0.056	56.1
41	64.84	11.4	11.3	11.3	1.01	1.01	1.02	14	14	15	0.098	56.4
42	65.84	11.5	11.1	11.3	1.00	1.03	1.01	14	14	14	0.15	56.6
43	66.84	11.4	11.4	11.1	1.05	1.02	1.00	14	15	14	0.073	56.8
44	67.84	11.4	11.4	11.6	1.04	1.02	1.03	14	15	14	0.079	57.0
45	68.84	11.4	11.5	11.5	1.05	1.02	1.01	14	14	15	0.056	57.2
46	69.84	11.4	11.6	11.5	1.04	1.00	1.04	14	14	14	0.055	57.4
47	70.84	11.4	11.6	11.5	1.02	1.01	1.02	14	14	15	0.094	57.6
48	71.84	11.7	11.3	11.6	1.00	1.03	1.03	14	14	14	0.095	57.7
49	72.84	11.6	11.6	11.6	1.03	1.04	1.02	14	14	14	0.042	57.9
50	73.84	11.6	11.6	11.7	1.03	1.01	1.01	14	15	14	0.046	58.1
51	74.84	11.7	11.9	11.8	1.03	1.02	1.02	14	15	14	0.046	58.2
52	75.84	11.7	12.0	11.6	1.02	1.04	1.01	14	14	14	0.046	58.4
53	76.84	11.8	11.7	12.1	1.01	1.03	1.03	14	14	15	0.095	58.5
54	77.84	12.1	12.1	11.9	1.01	1.02	1.03	14	14	15	0.10	58.7
55	78.84	12.0	12.0	11.7	1.03	1.02	1.01	14	15	14	0.12	58.8
56	79.84	11.9	11.9	11.9	1.03	1.02	1.03	14	14	14	0.087	59.0
57	80.84	11.9	12.1	12.1	1.02	1.02	1.01	14	14	14	0.095	59.1
58	81.84	11.9	12.2	12.2	1.03	1.03	1.03	15	14	14	0.087	59.2
59	82.84	12.0	12.1	12.1	1.03	1.03	1.01	14	15	15	0.095	59.4
60	83.84	12.1	12.1	12.1	1.03	1.04	1.02	15	14	14	0.13	59.5

Table D.10 – continued from previous page

test no	age [h]	unloading moduli [GPa]			unloading speed [kN/s]			number of data points			eccentricity [mm]	ξ [%]
61	84.84	12.2	12.1	12.1	1.02	1.02	1.00	14	14	14	0.083	59.6
62	85.84	12.2	12.1	12.1	1.00	1.03	1.02	14	14	14	0.079	59.7
63	86.84	12.2	12.1	12.2	1.02	1.02	1.04	14	14	14	0.089	59.8
64	87.84	12.3	12.0	12.3	1.03	1.02	1.03	15	14	15	0.05	60.0
65	88.84	12.4	12.3	12.3	1.01	1.01	1.02	14	14	14	0.093	60.1
66	89.84	12.3	12.4	12.2	1.08	1.04	1.03	13	14	14	0.05	60.2
67	90.84	12.5	12.2	12.2	1.00	1.02	1.04	14	14	14	0.068	60.3
68	91.84	12.6	12.2	12.3	1.01	1.04	1.03	14	14	14	0.076	60.4
69	92.84	12.4	12.4	12.2	1.04	1.03	1.02	14	13	14	0.028	60.5
70	93.84	12.5	12.5	12.2	1.04	1.04	1.02	14	14	14	0.089	60.6
71	94.84	12.6	12.5	12.4	1.03	1.02	1.03	14	14	14	0.088	60.7
72	95.84	12.3	12.6	12.6	1.03	1.04	1.02	14	14	14	0.087	60.8
73	96.84	12.5	12.4	12.6	1.04	1.03	1.02	14	15	15	0.088	60.8
74	97.84	12.5	12.6	12.4	1.01	1.00	1.04	14	14	14	0.068	60.9
75	98.84	12.6	12.6	12.5	1.01	1.05	1.01	14	14	14	0.064	61.0
76	99.84	12.5	12.7	12.7	1.02	1.00	1.03	14	14	14	0.064	61.1
77	100.8	12.5	12.7	12.8	1.04	1.04	1.01	14	14	14	0.087	61.2
78	101.8	12.4	12.5	12.6	1.02	1.02	1.04	14	14	14	0.13	61.2
79	102.8	13.0	12.6	12.7	1.02	1.05	1.02	14	14	14	0.14	61.3
80	103.8	13.0	12.5	12.7	1.03	1.03	1.02	14	14	14	0.10	61.4
81	104.8	12.6	12.9	12.7	1.01	1.01	1.03	14	14	14	0.12	61.5
82	105.8	12.6	12.5	12.7	1.01	1.02	1.02	14	14	14	0.10	61.5
83	106.8	12.7	12.8	12.7	1.02	1.03	1.02	14	14	14	0.064	61.6
84	107.8	12.8	12.9	12.8	1.03	1.03	1.02	14	14	14	0.057	61.7
85	108.8	13.2	13.0	12.7	1.01	1.02	1.02	14	14	14	0.076	61.7
86	109.8	12.8	12.7	12.8	1.03	1.05	1.03	14	14	14	0.14	61.8
87	110.8	12.9	13.1	13.1	1.03	1.03	1.03	14	14	14	0.14	61.8
88	111.8	13.1	12.8	12.9	1.03	1.02	1.02	14	14	14	0.14	61.9
89	112.8	13.1	13.0	12.7	1.08	1.03	1.03	13	14	14	0.10	62.0

Table D.11: Results from ultrasonics testing on a cement paste sample with $w/s = 0.42$ and $w/c = 0.50$, produced on Nov 11, 2013, at 11h00; six orthogonal diameters were measured as 30.0, 29.9, 29.9, 29.8, 29.9 and 29.7 mm

test no	age [h]	longitudinal wave speed [km/s]	shear wave speed [km/s]	dynamic Young's modulus [GPa]	ξ [%]
1	27.50	2.675	1.344	9.15	40.26
2	30.50	2.740	1.397	9.79	42.59
3	46.58	2.947	1.516	11.48	51.00
4	49.50	2.982	1.544	11.85	52.07
5	52.75	2.995	1.558	12.04	53.16
6	70.50	3.064	1.615	12.85	57.50
7	73.75	3.086	1.630	13.09	58.06
8	77.17	3.116	1.648	13.36	58.60
9	94.25	3.119	1.676	13.73	60.61
10	97.33	3.206	1.703	14.23	60.88

Table D.12: Results from ultrasonics testing on a cement paste sample with $w/c = 0.50$ and $w/s = 0.42$, produced on Nov 14, 2013, at 10h29; six orthogonal diameters were measured as 30.2, 29.8, 30.1, 29.8, 29.7 and 30.0 mm

test no	age [h]	longitudinal wave speed [km/s]	shear wave speed [km/s]	dynamic Young's modulus [GPa]	ξ [%]
1	27.77	2.736	1.360	9.40	40.49
2	29.43	2.763	1.384	9.70	41.81
3	47.52	3.058	1.480	11.19	51.35
4	52.77	3.196	1.505	11.65	53.17
5	95.35	3.270	1.726	14.75	60.71
6	97.52	3.259	1.743	14.95	60.89